Deltares

Morphological model for the River Meuse

Initial calibration of Grave-Lith v0.8

enabling delta life

foto: RWS/J.v.Houdt

Morphological model for the River Meuse

Initial calibration of Grave-Lith v0.8

Authors
Willem Ottevanger, Victor Chavarrias, Wout Leemeijer

Cover: View of the Meuse River.

Morphological model for the River Meuse

Initial calibration of Grave-Lith v0.8

Client	Rijkswaterstaat
Contact	Arjan Sieben, Roy Frings, Joey Ewals
Reference	SITO Programmasubsidie IenW 2024
Keywords	Meuse, Grave, Lith, D-HYDRO, SMT, morphology

Document control	
Version	1.0
Date	2024-12-18
Project number	11210364-002
Document ID	11210364-002-ZWS-0004
Pages	67
Status	final

Author(s)		
	Willem Ottevanger	Deltares
	Willem Ottevanger	

The allowed use of this table is limited to check the correct order-performance by Deltares. Any other client-internal-use and any external distribution is not allowed.

Doc. version	Author	Reviewer	Approver
0.1	Willem Ottevanger	Anke Becker	Johan Boon
1.0	Willem Ottevanger	Anke Becker	Johan Boon

Summary

The current report concerns the setup and calibration of the morphological model of the Meuse between Grave and Lith. The river stretch Grave-Lith is located between river-kilometre (rkm) 175 and rkm 202.

The river bed is important for many different river functions, as it influences water levels, determines the dimensions of the navigation channel, determines the stability of man-made structures (in and beside the river), and is important for habitats.

Knowledge how the river bed develops is important considering:
- Design of measures along the main channel (river training works and sediment management);
- Evaluation of the effect of measures (Rivierkundig Beoordelingskader);
- Aiding in the monitoring of pilot locations (river widening and deepening, eroding banks, ...);
- Long term system development considering different maintenance strategies.

Currently, there are a few options how to assess these developments, namely expert judgement, computation of equilibrium development for small scale measures in the winterbed of up to 5 km (WAQMORF, D-FAST MI) and since 2020 a Delft3D FM 1D model of the Meuse.

The development of a two-dimensional Delft3D FM model will extend and uniformise the available options to assess the river bed of the Meuse with that of the Rhine and allow for an easier implementation of measures, and at a finer resolution than in the Delft3D FM 1D model.

The model developments take place over the course of several years and started in 2023. The work carried out in 2023 is reported in Ottevanger *et al.* (2024a) and led to model version v0.5 (uncalibrated). The current report is a progress report that describes only changes or additions that were made in 2024 and resulted in model version v0.8 (partially 1D calibrated). Choices made in 2023 and 2024 may be changed in the following years to further improve model performance. Once the model of the entire Meuse is ready, a final report will be made that contains a full description of all data, methods and results used for the final version v1 of the model.

In the current report a method was refined to set up a submodel for the reach based on the 20 m Meuse grid and boundary conditions, initial conditions and weir settings from the 40 m hydrodynamic Meuse model. The approach was refined to align as much as possible with the current hydrodynamic models of the Meuse.

A data analysis of the bed level changes showed the importance of knowing the locations of dredging as well as the bed level changes caused by maintenance dredging. Using a schematised hydrograph between 2011 and 2021 a net reduction in bed material transport of roughly 10 000 m^3 (including pores) was found between rkm 176 and rkm 181 at a location where the main channel was lowered.

Using the above estimate, it was possible to make a first estimate of suitable parameters for the sediment transport formula. This choice was imposed in the simulation, which lead to a reasonable first estimate of the bed level changes for the reach.

Different recommendations for future steps are discussed, which include, assessment of the model sensitivity results to the initial bed levels, further one- and two-dimensional calibration.

Contents

List of Tables

List of Figures

1 Introduction

1.1 Background and Motivation

The riverbed (main channel and flood plains) of the Meuse supports many network functions as it influences water levels, determines the dimensions of the navigation channel, determines the stability of man-made structures (pipelines, cables, tunnels, bridges in and beside the river), and is important for habitats, and is to a degree source of natural resources (gravel and sand). The riverbed changes over time under the influence of morphological processes and human intervention. In the Rhine branches, morphodynamic evolution of the riverbed can be predicted and assessed with the so-called DVR model (Duurzame vaardiepte Rijndelta – Sustainable Fairway Rhine-Delta). In the Maas, no such two-dimensional morphodynamic model is available.

In order to make a morphological assessment for the Meuse river, there are the following options:

1 expert judgement,
2 computation of equilibrium development for small scale measures in the flood plains of up to 5 km using 5th generation WAQMORF (Mosselman, 2013; Van der Mheen and Prins, 2015),
3 usage of similar tool D-FAST MI for 6th generation, (Sieben, 2010; Jagers and Giri, 2022; Giri and Jagers, 2022) and
4 since 2020 a Delft3D FM 1D model of the Meuse (Berends *et al.*, 2020).

There are different reasons for development of a morphological model for the Meuse, namely:

- several important interventions have been completed or are under development (Maaswerken, Water Framework Directive),
- *Rijkswaterstaat* is moving to a new model generation in new software (the sixth generation models in the D-HYDROsoftware package) and the sixth generation hydrodynamic model of the Meuse (De Jong, 2021) is available for several years,
- there are new data and insights regarding morphological developments,
- *Rijkswaterstaat*is working on a similar model development in the Rhine branches to replace the DVR (Duurzame vaardiepte Rijndelta) models.

In addition, an up-to-date and reliable model is needed for river management issues such as:

- project design of interventions in/along the main channel (normalisation, sediment management),
- impact assessment for evaluation of measures (river engineering assessment framework (Rijkswaterstaat, 2023)/licensing),
- analyses of/after monitoring in pilots (sediment management, eroding banks, river widening such as by longitudinal dams, etc.),
- system analyses for long-term scenarios with management variants, e.g. for IRM (Integraal RivierManagement – Integrated River Management) so that estimates can be made of the morphological development on the different river functions.

In summary, the development of a two-dimensional Delft3D FM model will extend and uniformise the available options to assess the river bed of the Meuse with those of the Rhine and allow for an easier implementation of measures, and at a finer resolution than in the Delft3D FM 1D model.

1.2 Objective

The objective of this project is the development of a new modelling instrument that simulates the complex spatial riverbed dynamics in the Meuse river, enabling us to predict developments and effects of interventions in the riverbed, examine options for long-term (2050-2100) management and policy decisions, and thus shape the river management of the future.

1.3 This report

The goal of the current study is to improve the model in Ottevanger *et al.* (2024a) by performing a calibration on the period 2011-2021 which has higher discharges and covers a longer period than in the former period 2014-2018. It is expected that this will improve the calibration of the model. In addition, the choice of the steady state hydrodynamics simulations are better aligned with the existing practice in the development of the hydrodynamic models (cf. Van der Deijl (2023); Fujisaki *et al.* (2022)) including the contributions of lateral in- and out-flows.

Once the models for all reaches are finished completely, a series of final reports will be made as follows:

1. main report for all Meuse reaches together, summarising the definitive choices and results
2. calibration reports per reach
3. brief synthesis report, which summarizes, per Meuse reach, the information used in the model and what the model can be used for. This report needs to be easy to read, also by non-experts on morphological modelling.
4. manual, with sections on
   - a. tutorial for setting up a new model
     - i. how to change model input, if needed specified per reach or river section
     - ii. which input is the user allowed to modify, and which not
     - iii. how to use the available scripts for modifying input and for visualizing model output
   - b. how to apply the model in applications for permits (“vergunningaanvragen”) according to the “Rivierkundig Beoordelingskader (RBK)”
     - i. which hydrograph to use
     - ii. how many years to simulate
     - iii. which standard figures to produce and analyse
     - iv. etc.
   - c. how to apply the model for policy studies, such as “Integrated River Management (IRM)”
     - i. which hydrograph to use
     - ii. how many years to simulate
     - iii. which standard figures to produce and analyse
     - iv. etc.
5. factsheets, for use on the IPLO[1] website, via which model schematizations can be requested. These need to support the choice of model for a specific question.

[1] https://iplo.nl/thema/water/applicaties-modellen/modelschematisaties/

6 transfer protocol – “Protocol van Overdracht (PvO)” - the questionnaire to be answered before the model can formally become part of the official set of RWS models

1.4 Software

Within this project, the following software was used:

Table 1.1 Software versions used.

Software package	Version	Used for
D-HYDRO Suite	2.21.17.76916 (2023.01) 2.26.15.78894 2.26.26.79029 2.28.06 2.28.07	Hydrodynamic simulations Morphological simulations
Baseline	6.3.2	Schematization of model geometry
ArcGIS	10.6	In combination with Baseline

1.5 Historical background

The reach has undergone substantial changes in the past centuries. Figure 1.1 shows the old situation between Grave and Lith in 1892. The stretch was characterised by many bends. In the 1930’s, the plan of Lely (1926) was executed, which included many bend cut-offs. This lead to the Maas being able to convey more water than before. Ultimately, these river changes also lead to the closing of the Beersche Weir (in Dutch: Beersche Overlaat) in 1942 which was no longer necessary to prevent high flood levels along the Meuse. The extent of the inundation was also referred to the Beerse Meuse and is shown in Figure 1.2. An overview of these works is given in De Vries (1947). The current channel layout is shown in Figure 1.5.

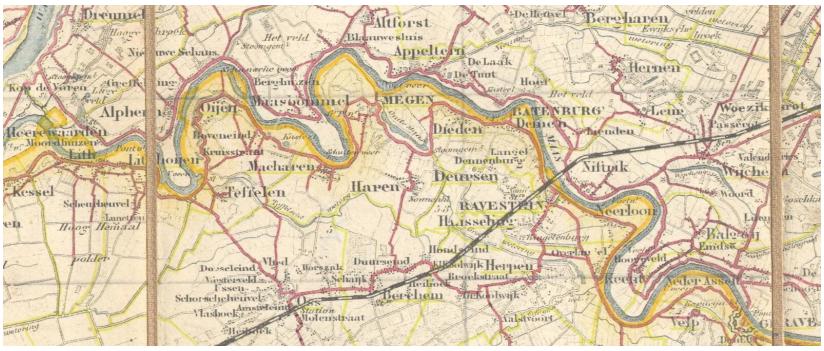

Figure 1.1 Topographic map of the Netherlands in 1892. Source: BHIC

Following the floods in 1993 and 1995, as part of the Maaswerken a main-channel bed-level lowering (in Dutch: *zomerbedverdieping*) took place between Grave and Ravenstein (cf. Figure 1.3). In addition different nature rehabilitation projects (Water Framework Directive (Kader Richtlijn Water, WFD)) took place in the reach between 2010 and 2021 (cf. Figure 1.4)

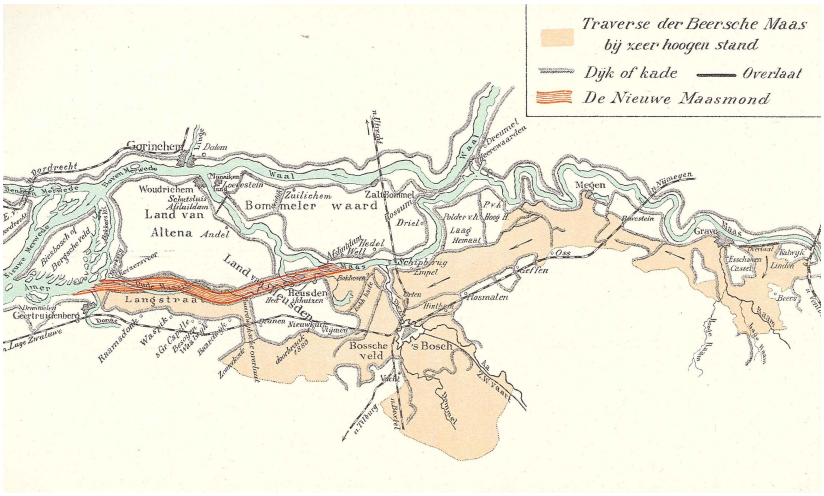

Figure 1.2 Innundation of the Beerse Meuse: Source: BHIC, The Beerse Meuse was a retention reach which could to be inundated since around 1400 to help reduce water levels along the Meuse.

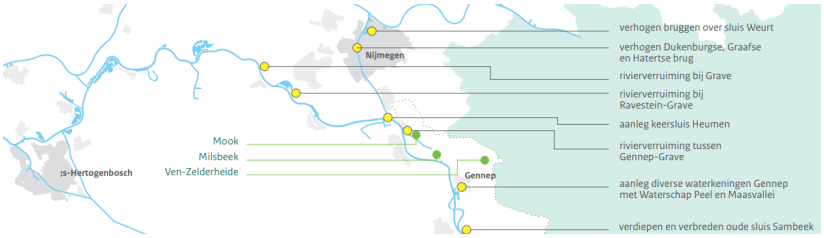

Figure 1.3 Overview of measures for the Maaswerken. Source: Rijkswaterstaat

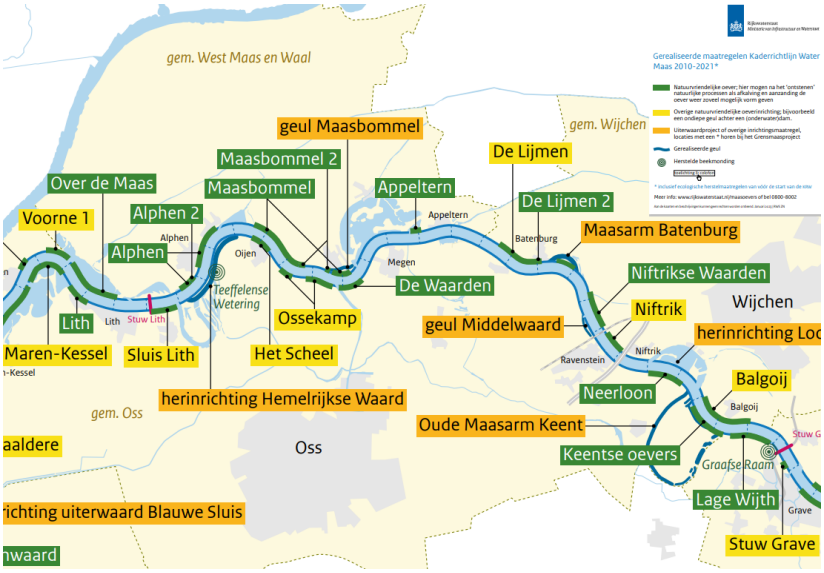

Figure 1.4 Overview of nature rehabilitation measures in the reach Grave-Lith. Source: Rijkswaterstaat

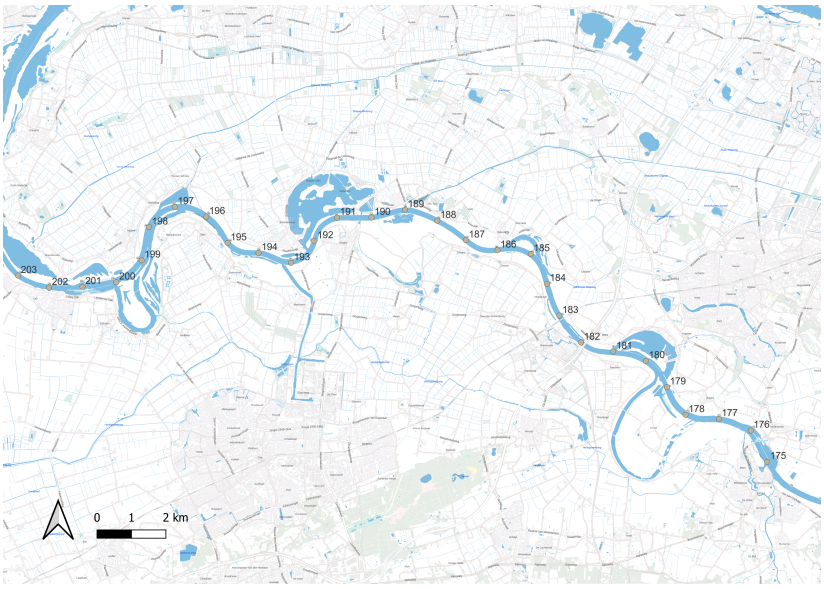

Figure 1.5 Overview of the current Grave-Lith reach (including the riverkilometres).

2 Approach for model setup

Spruyt and Ottevanger (2019) developed a plan of action for the development of the morphological model for the Meuse. Based on this, they present a general approach, which foresees a model development in several steps. These steps are extended as follows for this project:

- v0 This version is a basic model that contains the most important functionality, with the main goal to have a running but not yet too complex model.
- v1 Building on v0, the first model version is a version which covers similar functionality as is provided for the Rhine by the existing DVR (Duurzame Vaardiepte Rijndelta) model. Moreover, the model is based on the latest available data and insights.
- v2 The second model version is based on v1 but extended with new functionality to make the model suitable for more types of applications (e.g. finer grids, exchange of sediment between main channel and flood plains, bank erosion processes, etc.).
- v3 The third model version is used to develop new insights and functionality.

Table 2.1 shows the development of the model according to the different phases and an overview of the progress in the past years.

2.1 Background

The hydrodynamic model set up by De Jong (2021) includes the Meuse from Lixhe to Keizersveer. Different weir operations are incorporated in the model. Moreover to calibrate the model different model versions have been setup. These represent the river geometry in the years 1995, 2012, 2014 and 2019. In these years, different floods occurred which enable the validation for the high-discharge events. Recently Van der Deijl (2023) also applied the hydrodynamic model for a hindcast of the flood wave of July 2021.

2.2 Activities prior to 2024

An initial model was set up by Ottevanger *et al.* (2020).

In 2021, a pilot reach in the Common Meuse (in Dutch: Gemeenschappelijke Maas, also Grensmaas) was identified near Meers. The location of Meers was modelled by carrying out multiple simulations. The current status of the Meers model is that there are still differences in the results between sequential and parallel runs. Although many runs were performed and different software bugs were resolved, the differences remain at this location. It is hypothesized that the inherent sensitivity of the system (geometry, mathematical formulations and the numerical translation thereof) lead to differences which can be large with respect to an initial perturbation.

Since 2022, the reach of Sambeek-Grave was selected as a second pilot location. This location is well suited as there is a large-scale measure (summer-bed lowering) which has been implemented and the bed level is measured every year. Moreover, the reach has a lower slope and it appears that models of low-slope rivers are found to be less sensitive, compared to the steeper river reaches like the Meers model. This is demonstrated by findings in a model of the Western Scheldt and different schematic river models.

In 2023, the Sambeek-Grave reach was finalised at version 0.8, in which the sedimentation in the summerbed lowering was used as a calibration parameter. Between Linne and Keizersveer different submodels were generated at version 0.5, using the sediment transport settings of the Sambeek-Grave model. The models all used the discharge sequence between 1-6-2014 and 1-6-2018. Unfortunately, during this period there were not very large discharges, which implies, that it is difficult to judge how representative the models are for higher flood discharges.

2.3 Overview of the activities

Table 2.1 describes the model development steps per sub-category, and the present status of the different reaches of the Meuse. For legibility the following abbreviations have been introduced:

- EK: Eijsden-Keizersveer,
- LiK: Lixhe-Keizersveer,
- ML: Monsin-Lixhe,
- LB: Lixhe-Borgharen,
- BL: Borharen-Linne,
- LR: Linne-Roermond,
- RB: Roermond-Belfeld,
- BS: Belfeld-Sambeek,
- SG: Sambeek-Grave,
- GL: Grave-Lith,
- LK: Lith-Keizersveer.

Table 2.1 Steps in model development

activity areas	associated activities	model version	2020	2021	2022	2023	2024
data collection	• Collection of all data needed to set up a model, e.g. boundary conditions, calibration data hydrodynamics and sediment transport and morphology, bed composition, etc.	v0,v1	EK - v0, Meers - v0	SG	SG, Li-K	SG v0.8, LR v0.5, RB v0.5, BS v0.5, GL v0.5, LK v0.5	GL v0.8
morphodynamic model schematization: towards a well-working basic model (v0)	• set-up of a first running model including: a. dynamic river bed b. representative initial bed elevation (e.g. smoothing of bed forms) c. suitable roughness formulation for morphology d. sediment (grain sizes and sediment layers, with focus on active/upper layer) e. secondary flow f. first choice of transport formula and parameters (uncalibrated) g. non-erodible and less erodible layers h. suitable grid resolution	v0		 SG SG - v0.5 EK EK	 SG - lokale 20 m	 SG LR, RB, BS, GL, LK - 20 m	 GL, BL GL GL, BL

(continues on next page)

Table 2.1 – continues from previous page

activity areas	associated activities	model version	2020	2021	2022	2023	2024
	• testing phase v0 model, identification of problems and modification of the schematization accordingly						Adding sluices as weirs at Linne and Born
extending the basic model to a v1 model	• more sophisticated description of a. main channel roughness b. composition and thickness of underlayers, including non-erodible layers • set-up of a dredging and dumping module • testing phase v1 model, and iterative modification of model schematization if necessary	v1			 SG	 (sed.trans. including separate roughness) SG (fully mobile)	 GL, BL, constant Chezy
development of methodologies and tools for running the model	• approach and tools for model simulation (i.e. Simulation Management Tool) • strategy for model spin-up • strategy and tools for model evaluation and presentation of results • strategy and tools for simplification of model set-up and improving reproducibility	v0,v1	 EK, EK - v0	 SG - Too coarse	 SG - Local 20 m	 Improvement of restart to seconds Submodels based on standard simulations Start on user manual	 Connection to standard discharge simulations
model calibration and validation	• calibration and validation strategy • adapting the hydrodynamic model to make it suitable for morphodynamic simulations • hydrodynamic validation • *offline* calibration giving a first estimate of morphological response based on the flow field in the hydrodynamic simulations • 1D morphodynamic calibration and validation (focusing on width-averaged, large-scale and long-term trends)	v1		2014-2018	2014-2018 remove weirs 50000 m3/year, Influence of fixed layers	2014-2018 20 m submodels SG v0.8, LR v0.5, RB v0.5, BS v0.5, GL v0.5, LK v0.5 Jump at SG lowering Analysis of statistical output of bed level changes	

(continues on next page)

Table 2.1 – continues from previous page

activity areas	associated activities	model version	2020	2021	2022	2023	2024
	• 2D morphodynamic calibration and validation (focusing on 2D patterns in the river bed, such as bar patterns and bend profiles) • validation of dredging and dumping module						
exploring model uncertainties	• influence of unknown physical variables (e.g. roughness in transport, bed composition, active layer thickness) • influence of model settings (e.g. initial geometry/composition and boundary conditions) or modelling concepts (e.g. Hirano model) • influence of simulation strategy and approaches (e.g. methods for optimizing simulation time, schematization of the hydrograph, choice of simulation period)	v1-v3					
development of modelling strategies and development for future use of the model	• identifying types of application and requirements • development of strategies for application of the model (e.g. choice of scenarios, choices • for model settings and geometry, type of interventions) • identifying needs for further development of the model schematization (including needs for knowledge development and data requirements) • implementation and testing	v1-v3					
verification of model application	• testing the model application in test cases of a. effect of interventions b. planning study (*planstudie*) c. (long-term) forecast of system behaviour • improvement of the model schematization, modelling strategies, methodologies and tools based on the outcomes of the test cases	v1-v3					
implementation of new functionality in D-HYDRO reports	• identifying requirements of new functionality • functional design of needs • design of implementation • implementation and testing • updating user manuals	v2-v3	Ottevanger *et al.* (2020)	Ottevanger *et al.* (2021); Ottevanger (2021)	Ottevanger and Chavarrias (2022a,b)	Ottevanger *et al.* (2024a,b)	

(continues on next page)

Table 2.1 – continues from previous page

activity areas	associated activities	model version	2020	2021	2022	2023	2024
related work			Berends *et al.* (2020)	Chavarrias (2021)	Chavarrias and Ottevanger (2022)	Ottevanger (2023); Ottevanger and Chavarrias (2023); Van der Deijl and Ottevanger (2023); Van der Deijl (2023)	Fujisaki *et al.* (2022)

3 Model setup

3.1 Overview

For the development of the model the large scale model of De Jong (2021) is used as a basis. This model is based on the Baseline schematisation j21_6-v1. The construction of the model is similar to Ottevanger *et al.* (2024a), but is based on a later period (2021) in time and some discrepancies with respect to the earlier version are now resolved. In this report, differences related to this main setup are explained.

3.2 Structures

The water level in the reach between Grave and Lith is strongly influenced by the operation of weir Lith, which has to maintain specific water levels for navigation. For low discharges until 800 m^3/s the water level at Lith boven is maintained at 4.90 m + NAP by adjusting the gates at Lith. For discharges between 800 and 1250 m^3/s, a water level of 5.40 m + NAP at Megen dorp is used as a set point, while for discharges higher than 1250 m^3/s the set point is a water level of 3.95 m + NAP at Lith boven. This can be seen in Figure 3.1. Figure 3.2 shows the approximate corresponding discharges for the weir operation.

Within the reach there are different bridge crossings:

- MA_175.65_N324-John-S-Thompsonbrug-Grave
- MA_181.87_A50-Maasbrug-Ravenstein
- MA_182.87_Spoorbrug-Edithbrug-Ravenstein

The most upstream of these bridge crossings coincides with the location of the weir at Grave.

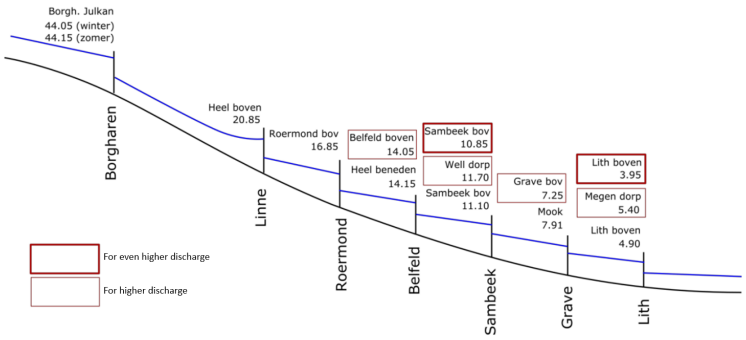

Figure 3.1 Water levels for weir operation on the Meuse (adapted from De Jong (2021))

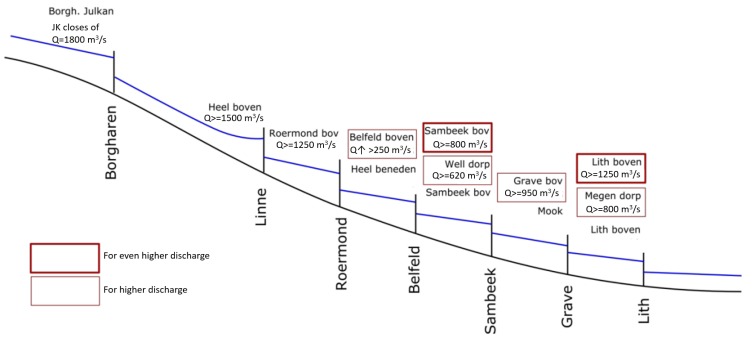

Figure 3.2 Discharges associated with the steering water levels for weir operation on the Meuse (adapted from De Jong (2021))

3.3 Grid

At some locations the morphologically active portion of the grid only covered three grid cells in the transverse direction (cf. Ottevanger *et al.* (2020)). In the Sambeek-Grave reach a locally refined grid was generated in the main channel (Ottevanger *et al.*, 2024b). Later, it was considered (Ottevanger *et al.*, 2024a), that aligning to the existing 20 m models developed by Fujisaki *et al.* (2022) was a more sustainable choice, also because the hydrodynamics of these models had undergone more scrutiny during the setup. The current model also builds forth on this choice. A small stretch of the used 20 m grid is shown in Figure 3.3.

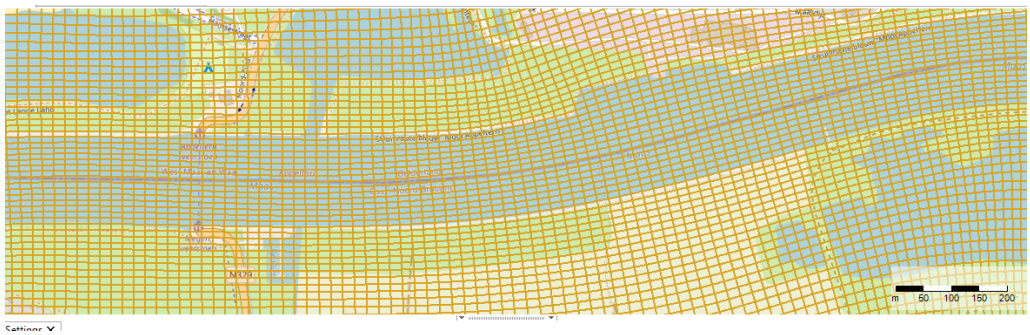

Figure 3.3 Example of the 20 m grid near Megen

3.4 Bed level

As the model is intended for calibration purposes, the bed level is based on the 2021 situation prior to the July 2021 flood. For details about the j21 Baseline schematisation see Van der Deijl (2023). Furthermore the bed levels are averaged from corner points (as in the standard hydrodynamic simulation) to the cell centre. In the main channel the bed level was imposed by a nearest neighbour interpolation from the measured multibeam data of 2011.

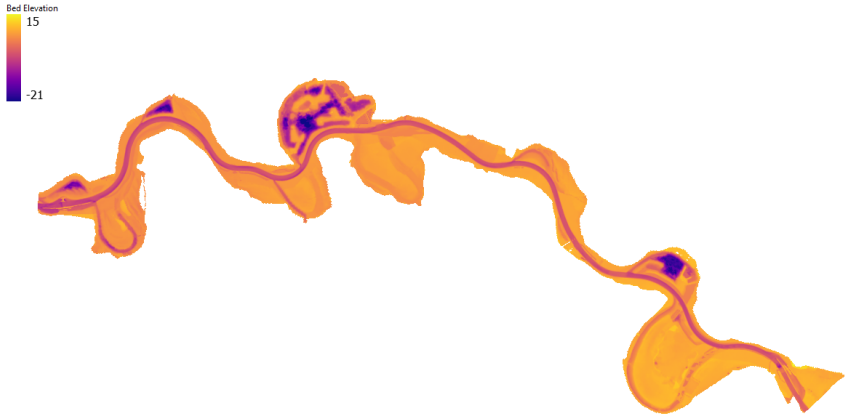

Figure 3.4 Bed level at the start of the simulation (considered to be at 31-12-2011)

3.5 Sediment properties

The sediment distribution was obtained from the 10 km moving average data set (Frings, 2022). This was interpolated along the channel, and extended uniformly in the tranverse direction. The various sediment classes that are used in the model are shown in Table 3.1. The sediment distribution as imposed in the model is based on Figure 3.5. The geometric mean grain size is shown in Figure 3.6.

Table 3.1 Overview of sediment classes.

Sediment fraction	Minimum diameter [m]	Maximum diameter [m]	Classification
Sediment1	6.30e-05	2.50e-04	sand
Sediment2	2.50e-04	5.00e-04	sand
Sediment3	5.00e-04	1.00e-03	sand
Sediment4	1.00e-03	2.00e-03	sand
Sediment5	2.00e-03	2.80e-03	gravel
Sediment6	2.80e-03	4.00e-03	gravel
Sediment7	4.00e-03	8.00e-03	gravel
Sediment8	8.00e-03	1.60e-02	gravel
Sediment9	1.60e-02	3.15e-02	gravel
Sediment10	3.15e-02	6.30e-02	gravel
Sediment11	6.30e-02	1.25e-01	gravel

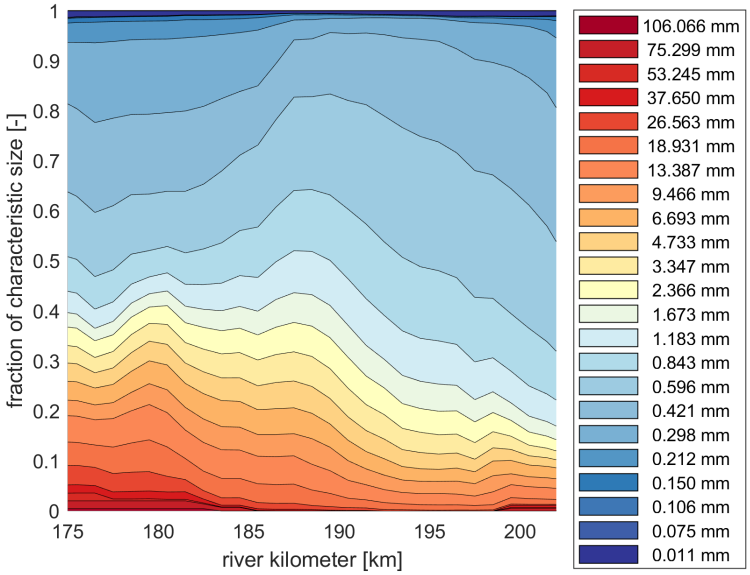

Figure 3.5 An overview of the fraction distribution as obtained from Frings (2022)

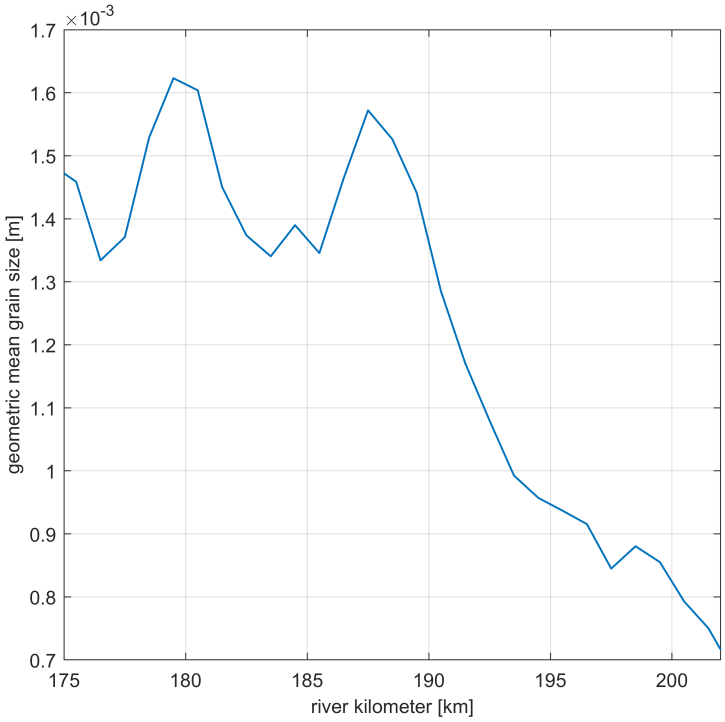

Figure 3.6 An overview of the geometric mean grain size as derived from Frings (2022)

3.6 Sediment availability

The sediment availability was limited to the L3R3 polygons (Meijer, 2020b,a). Besides that fixed layers were imposed, based on the information provided by *Rijkswaterstaat* Zuid-Nederland. The processing of the fixed layers was done by a QGIS Python processing script, which used different spatial layers of available and not available sediment locations. These layers are no longer combined into a single layer as the polygon-polygon intersection algorithms can take very long. The current approach uses the grid cell centre coordinate to determine whether it falls in different polygon locations. For the current derivation of the fixed layer locations the following files provided by *Rijkswaterstaat* are used:

- vOever
- vBodem
- hardelagen_bestortingenTEM

Figure 3.7 shows the availability of sediment in a near the fixed layer of Niftrik. An overview of the full reach is shown in Appendix A

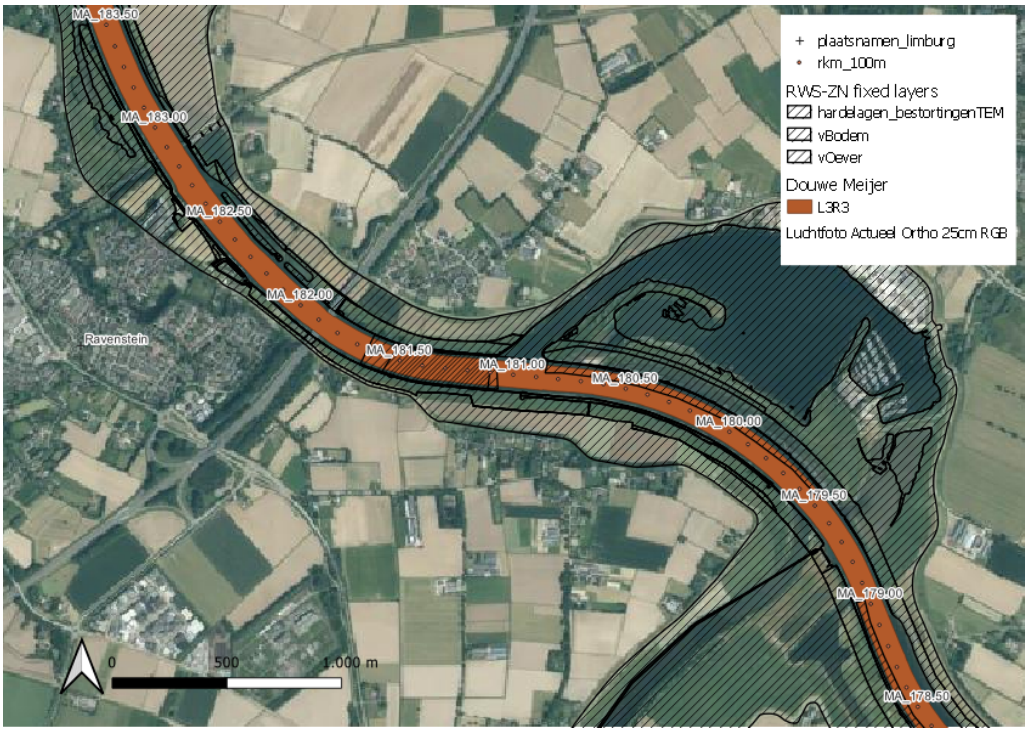

Figure 3.7 Sediment availability in the Grave-Lith reach near Niftrik. The brown shaded area is the location in which sediment is potentially available, and the arched areas the areas which are considered to be fixed. For example. at rkm 181-181.5 which is the fixed layer at Niftrik, this works out to no available sediment.

4 Hydrodynamic model preparation

In this chapter different steps are performed to arrive at a hydrodynamic model which is suitable for running the morphological model.

4.1 Discretization of the hydrograph

A schematic discharge wave is created for use with the simulation management tool (SMT, cf. Yossef *et al.* (2008); Ottevanger *et al.* (2020)). The approach used is similar to Yossef *et al.* (2008), in which the hydrograph is modelled through a set of constant discharge simulations with varying morphological factor, rather than a dynamic hydrograph.

For the reach Grave-Lith, there are bed level measurements available in the period between 31 December 2008 and 31 December 2023. The raw discharge measurements from measurement location Megen Dorp for this period are shown in Figure 4.1.

To run the morphodynamic model with the simulation management tool (SMT), first a discretization of the hydrograph needs to be made. This is done by using the following discharges: 50, 250, 500, 750, 1000, 1300, 1500, 1700, 2100, 2500, 2800 and 3200 m^3/s. The measured discharges at Megen Dorp are shown in Figure 4.1. First the discharges are resampled to day averages and subsequently rounded to the nearest representative discharge level, in terms of sediment transport capacity, under the assumption that sediment transport scales with the discharge to the power 5/3 (which holds for the formulation of Engelund and Hansen (1967)), (cf. Section 8.1 in Becker *et al.* (2023)).

Since the bed level data set of the Meuse has a larger coverage of the Meuse starting from 2011, the hydrograph is made with the discharges starting from 31 December 2011, meaning the period between 31 December 2008 and 31 December 2011 is left out. The morphodynamic simulation will run until and including the flood event in 2021, so that the calibration also includes this event, resulting in a hydrograph between 31 December 2011 and 5 August 2021. The resulting hydrograph is shown in Figure 4.2.

Next, to speed up the morphodynamic simulations even more, the peak discharges are determined for every year. All discharges above 500 m^3/s are considered to be peak discharges. For the discharge level of 500 m^3/s and lower the time durations before and after the peak discharge are combined, so that there are less transitions between the discharge levels in the hydrograph. This speeds up the simulation as the hydrodynamic spin-up time before the start of each morphodynamic computation is done less often.

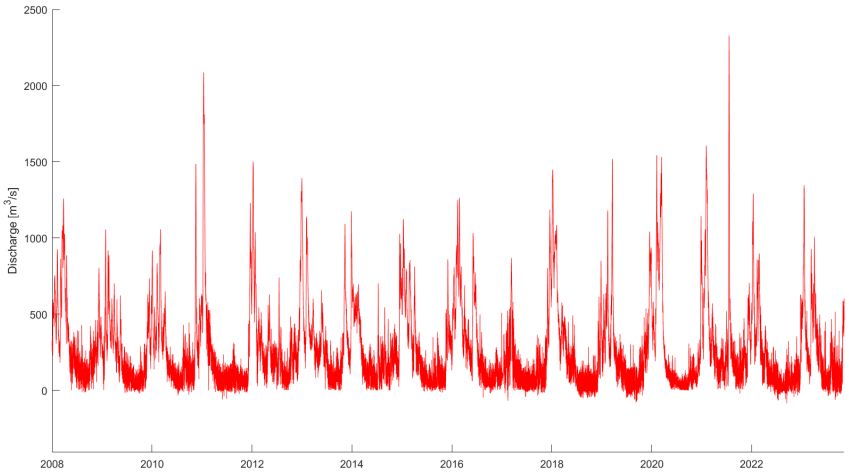

Figure 4.1 Discharge at Megen Dorp between 31 December 2008 and 31 December 2023.

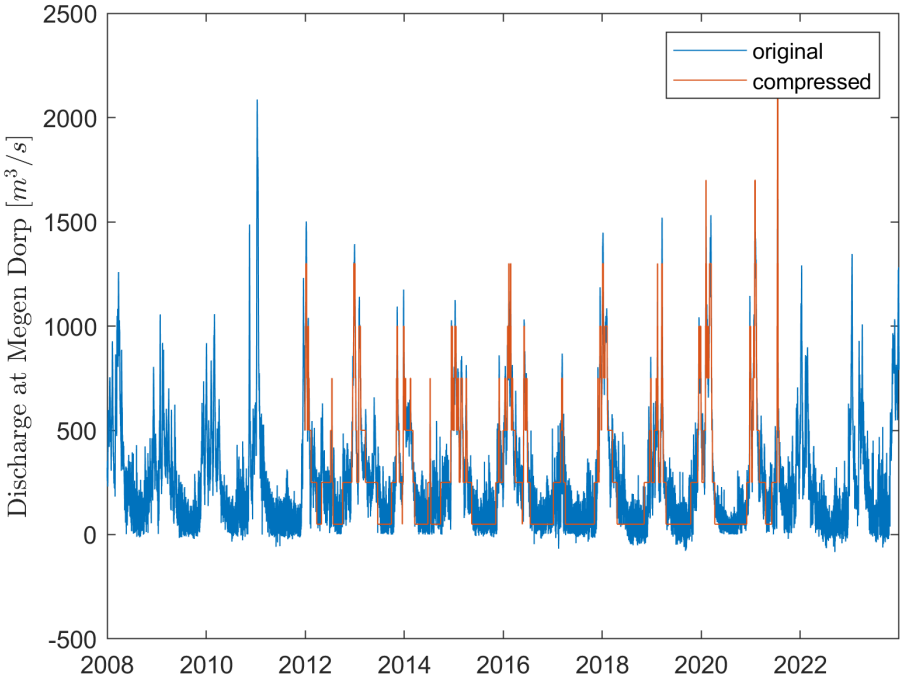

Figure 4.2 Discretised hydrograph using the most used discharges between 31 December 2011 and 5 August 2021.

Finally, different morphological factors were applied to the different periods. The SMT approach allows for a strong reduction in the computational time as different morphological acceleration factors can be used, depending on the discharge. Table 4.1 shows an overview of the imposed morphological factors. During the low flow period the bed level changes are considered to be small, and therefore larger MORFAC can be used. At the peak discharges a smaller MORFAC is used. For the 50 m^3/s discharge level the morphological factor is much higher than for the other discharges. During this period there is no composition or bed update. It has been included to ensure that the morphological time frame is easier to process. The sensitivity to the MORFAC in these simulations should be investigated further, and this could possibly lead to a further reduction of the simulation time.

Table 4.1 Overview of morphological factor per discharge.

Discharge [m^3/s]	MORFAC
50	1440
250	40
500	40
750	10
1000	5
1300	1
1700	1
1900	1
2100	1
2500	1
2800	1
3200	1

This results in the following distribution of discharges depending on the computed hydrodynamic time as shown in Figure 4.3. This shows that the morhpodynamic simulation time of 10 years has been reduced to a hydrodynamic simulation time of less than 80 days.

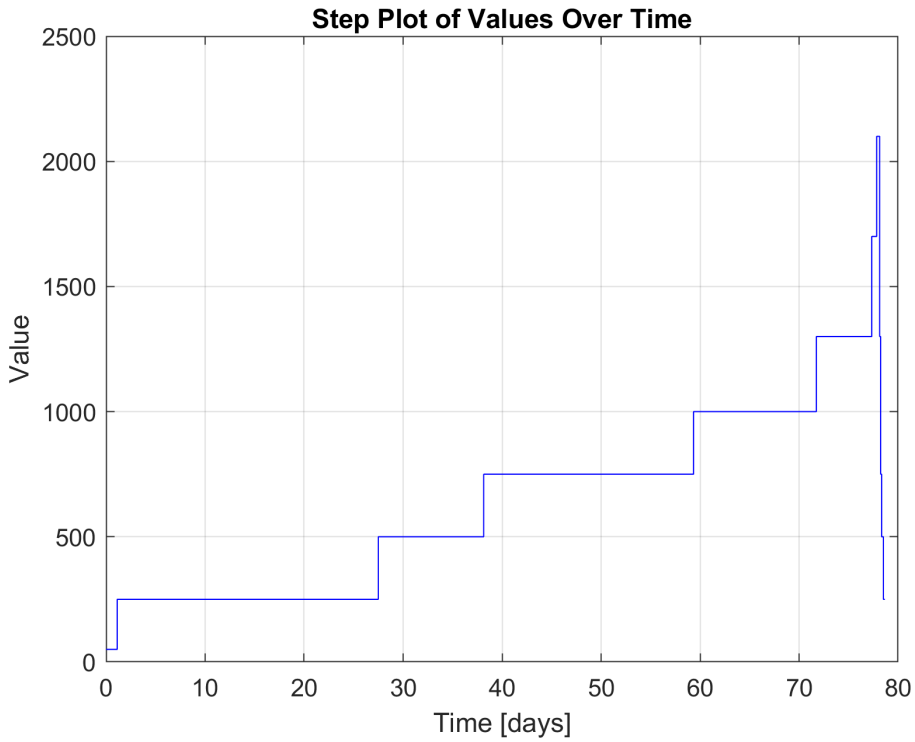

Figure 4.3 Schematic hydrograph using the selected set of discharges, with combined durations and applied MORFAC.

4.2 Initial simulations using the 40 m model

The 40 m model is based on the Baseline j21 schematisation (cf. Factsheets Delft3D FM Maas), which was derived particularly for the hindcast of the floodwave in July 2021 (Van der Deijl, 2023). Lateral discharges are derived in the model using the Boundary Condition Generator for Hydrodynamic Models (RGWM 2.4). The standard stationary discharges that are used in the hydrodynamic schematisations are used, as these specific discharges have been computed more often. It is expected that this is likely to lead to results which have been checked in more detail in previous years, and reduces the possibility for unexpected model results.

The stationary discharges which are chosen are S50, S250, S500, S750, S1000, S1300, S1500, S1700, S2100, S2500, S2800 and S3200. The letter S implies that it is a stationary simulation, and the number represents the discharge at Eijsden (approximately). The exact values can be found in the Factsheets Delft3D FM Maas.

Although the schematisation was available, these specific simulations were derived and run for a first time. Some checks of the outcome were done to check for instance that the water level followed a logical pattern depending on the upstream discharge. Figure 4.4 shows that the waterlevel along the channel shows a logical progression for the various discharges.

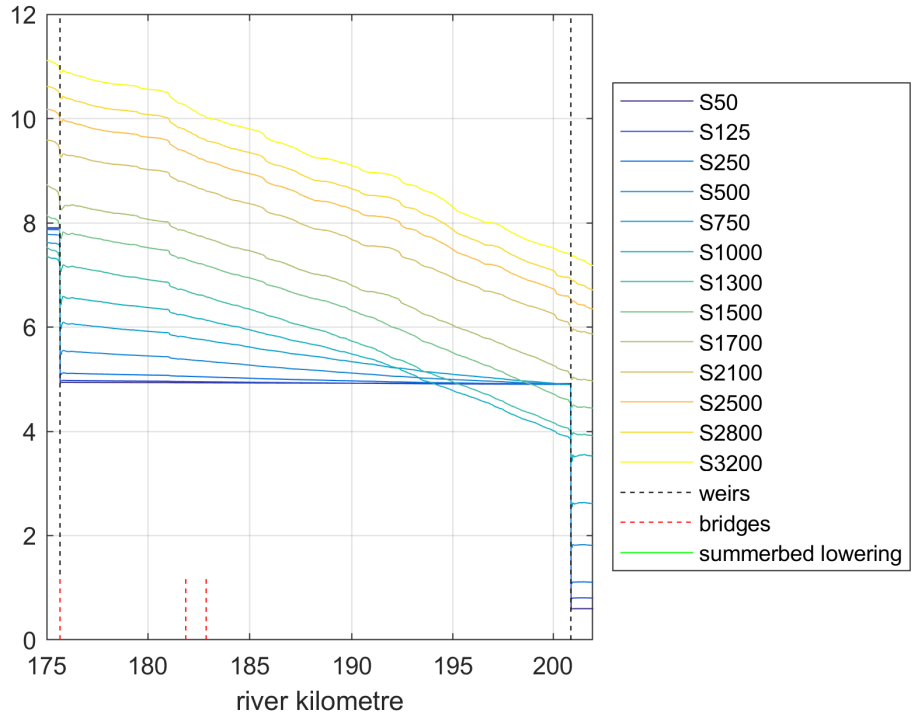

Figure 4.4 The water level for various discharges using stationary j21 simulations along the Meuse

Furthermore, the stationarity of the simulation was assessed. Figure 4.5 shows the water level change in the last two outputs of the hydrodynamic spinup simulation. This shows that, with the exception of the S50 simulation, in all simulations all water level variations are within 5 mm. For the purpose of the morphological simulation, we consider that this is an acceptable result. At the lowest discharge 50 m^3/s the differences are larger, but we expect that the morphological change at this discharge is limited. The main reason, that this was left was that the convergence of the S50 level was very slow, the current simulation was run for 12 days and as the final result was comparable to the set point level, we decided to accept this result, to move forward towards the 20 m grid simulations.

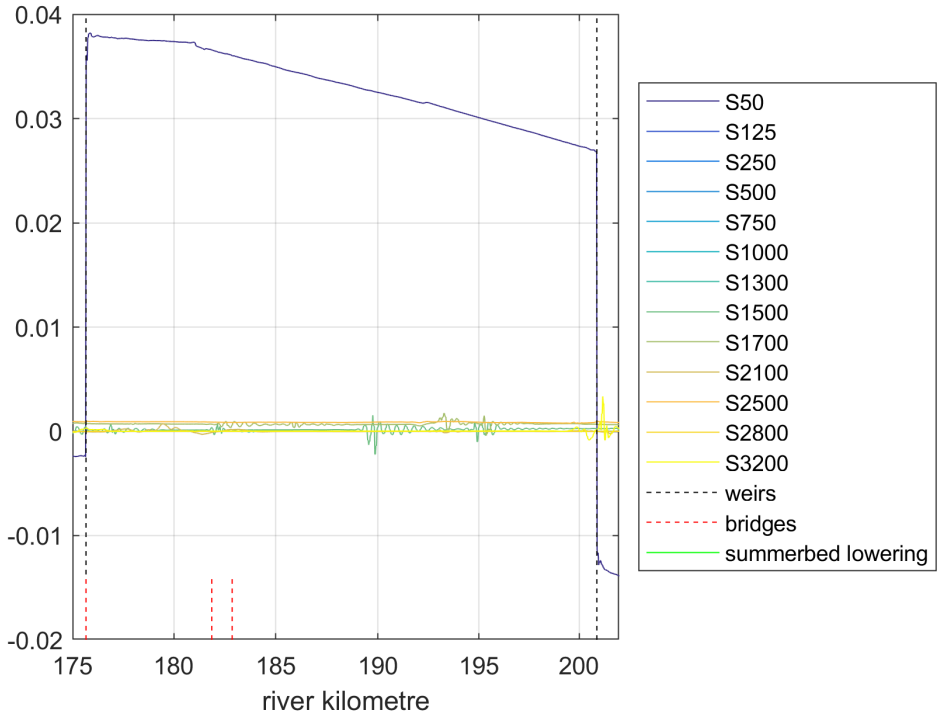

Figure 4.5 The water level difference for various discharges for the final two output times, using stationary j21 simulations along the Meuse

4.3 Preparation of the 20 m model

The 20 m model is now derived from Baseline, and boundary conditions, weir settings and initial conditions are derived. This is described in more detail in this paragraph.

Fujisaki *et al.* (2022) derived three refined grids (20 m) for the upstream, middle and downstream reaches of the Meuse. For the current project, a Baseline projection was done for these grids using the j21 model. Using model enclosures, reaches were shortened further. In this case the reach was shortened to the reach between Grave and Lith (using the downstream grid of Fujisaki *et al.* (2022)).

Along the model enclosure the discharge and a water level was derived on the basis of the 40 m results. Initially, the models were clipped to align exactly with the structure location. This however lead to inaccurate results compared to the 40 m model. Moreover, it proved to be challenging to obtain a boundary location which nicely aligned to the weir, while keeping all zones which are physically connected to the upstream water level as well (cf. Figure 4.6).

As a consequence the decision was made to move the upstream boundary location to upstream of the weir, and the downstream location to downstream of the weir (cf. Figure 4.7). This meant that now the weirs at Grave and Lith had to be included in the model as well.

To reduce the complexity for the morphodynamic model, the interaction with weirs steered by D-RTC Real Time Control was excluded from the model. Instead, the crest level of the weir is obtained from the steady state simulations of the 40 m model, averaging over a period of eight hours to account for possible oscillations in the crest height. The crest height of the weir for each discharge level can be seen in table 4.2.

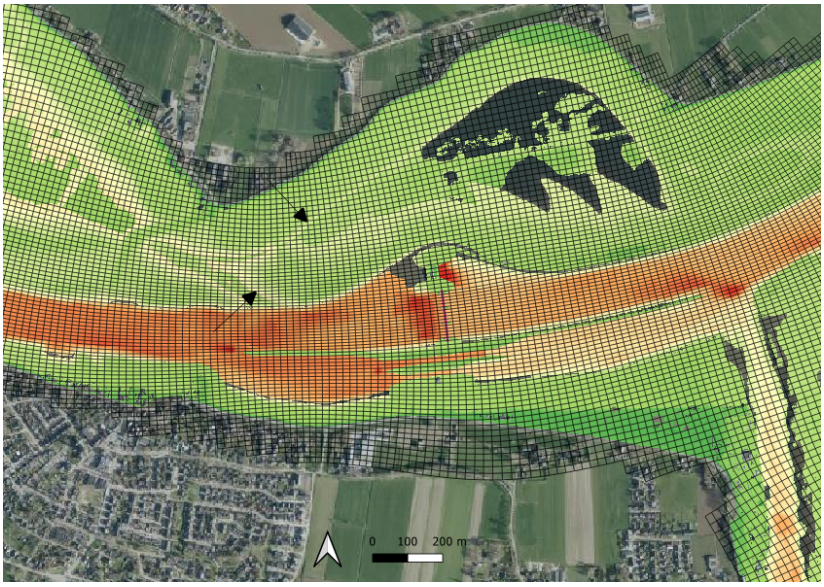

Figure 4.6 20 m grid super imposed on the bed elevation at Lith. The magenta line indicates the position of the weir at Lith. The arrows indicate downstream locations which are flow obstructing at medium discharges.

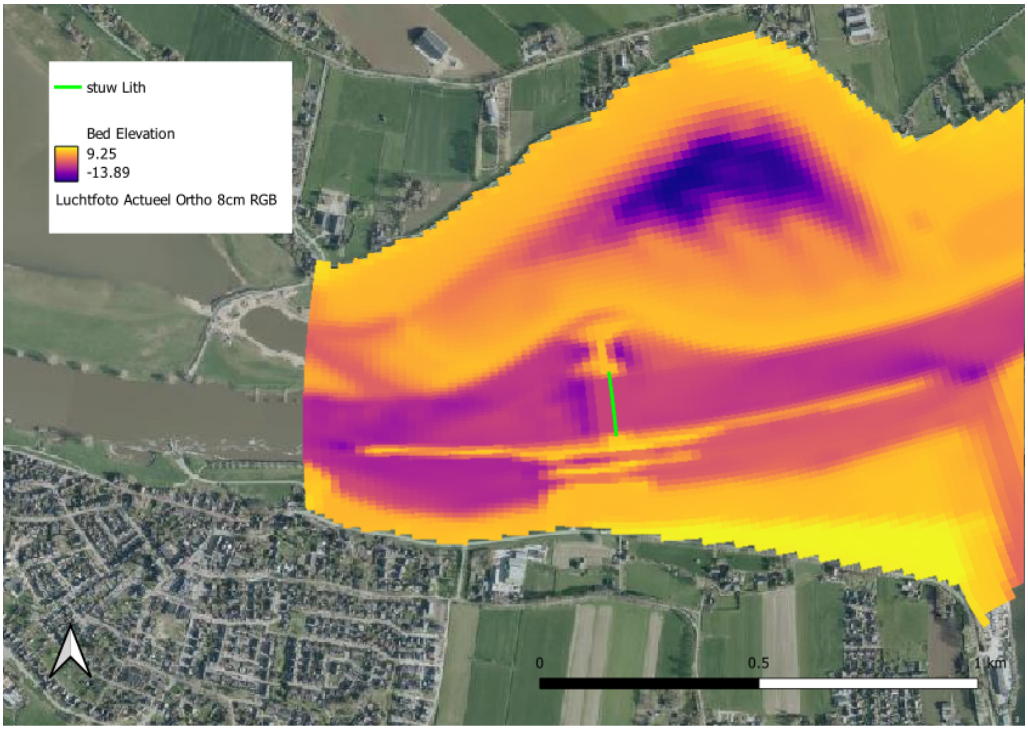

Figure 4.7 Extent of the model at Lith, extending to downstream of the weir of Lith.

During the first iterations of the model, leaks were discovered near the sluice at Lith. The sluice doors, were not included fixed weir file. Hence, in the 20 m model, the water could freely flow through the sluice, even for low discharges. To solve this now fixed weirs were added with the setpoint of the weir as the crest level height. In the 40 m model, the sluice location was blocked, due to the low horizontal grid resolution. A local improvement of the input was made (see Figure 4.8), but in the long term it is recommended to i) check the schematization at all weirs in the Meuse to see if more potential leaks are present, and add the sluice as a gate and possibly a pump as a measure for the next Baseline schematization of the Meuse model.

Table 4.2 Overview of the crest levels of the weir near Lith per discharge.

Discharge [m^3/s]	Crest Level [m]
50	4.15
125	3.83
250	3.40
500	2.71
750	2.13
1000	1.30
1300	-2.50
1700	-2.50
2100	-2.50
2500	-2.50
2800	-2.50
3200	-2.50

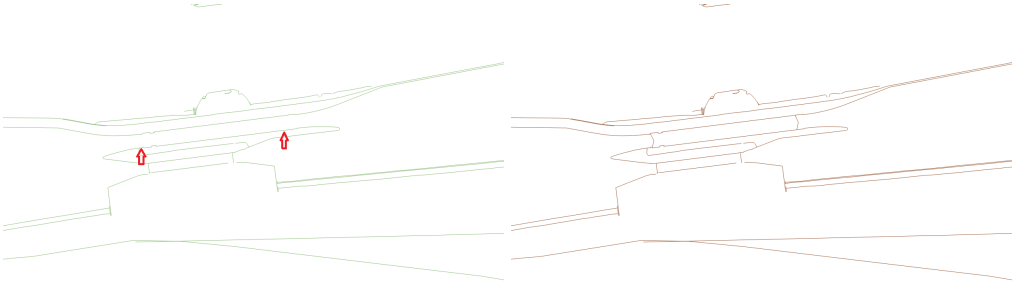

(a) No sluice doors

(b) Added sluice doors

Figure 4.8 Fixed weirs near sluice Lith a) without and b) including the sluice doors at Lith to the weir input file. The red arrows indicate the missing sluice doors.

For the initial fields of the water level and velocity, these are interpolated using the result of the 40 m model. To enable a field filling interpolation of the 40 m results, nearest neighbour interpolation with a relative search grid cell size of 2 is used.

Since the model could crash due to high flow velocities near the downstream boundary, another improvement has been made to the model. This is done by changing the downstream boundary conditions. Instead of per cell using a different water level value, causing differences between the water level in each boundary cell, all boundary cells are given the same value. This value is the average water level in all wet cells for each discharge level. The water level at the boundary for each discharge level can be seen in Table 4.3.

However, it turned out that for each discharge level some of the boundary cells are close to dry in the 20 m model. In such cases what could occur was a free flowing outflow if water levels temporarily exceeded the bed level in the cell near the boundary, leading to very high velocities locally, which subsequently lead to unstable flow fields and very small time steps. Therefore, new weirs with a crest level of 999 m are added in front of these cells, to prevent water from flowing past there. For a discharge of 1300 m^3/s the new boundary is shown in Figure 4.9. Since the water level at the boundary differs for each discharge level, the amount of dry and wet boundary cells differs as well. Hence, for each discharge level a different set of weirs is implemented.

Table 4.3 Overview of the downstream boundary water levels per discharge level.

Discharge [m^3/s]	Water Level [m]
50	0.60
125	0.81
250	1.11
500	1.82
750	2.63
1000	3.55
1300	3.94
1700	4.99
2100	5.90
2500	6.39
2800	6.77
3200	7.24

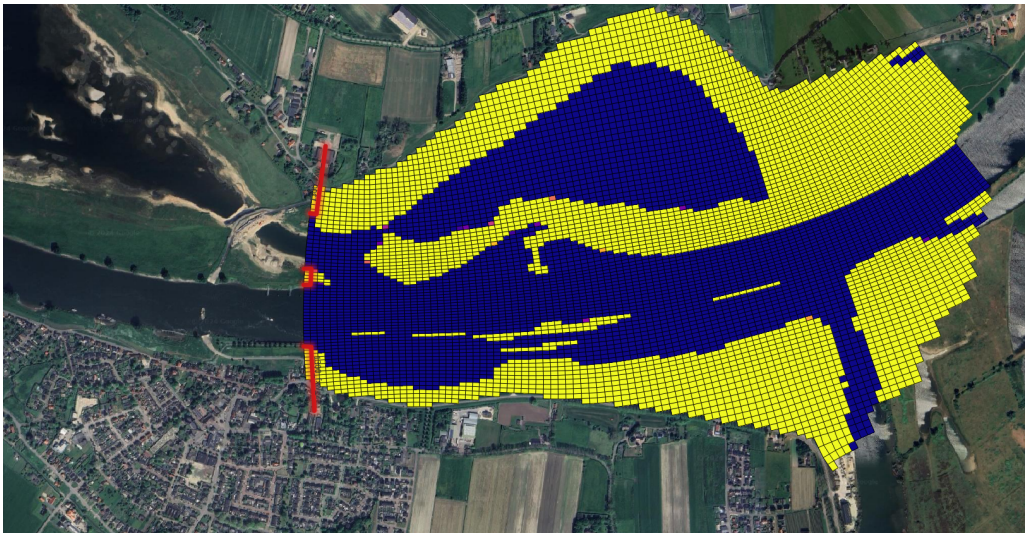

Figure 4.9 Updated downstream boundary for a discharge of 1300 m^3/s. The blue cells are the cells containing water and the yellow cells are the dry cells. The red line indicates the locations of the added weirs.

4.4 Comparison of 20 m and 40 m model

Figure 4.10, Figure 4.11 and Figure 4.12 show the water level for the 20 m model compared to the 40 m model. The sixth generation hydrodynamics models have their bed levels defined in the grid corner points. Morphodynamic models, however have the bed levels defined at grid cell-centre points. As the hydrodynamic models have been calibrated on the water levels, these are used as a starting point for the comparison of the 20 m models.

In the following graphs three discharges conditions namely 50 m^3/s (S50), 1300 m^3/s (S1300) and 3200 m^3/s (S3200) are compared for three different hydrodynamics models namely, the 40 m model with bed level at corners (40 m), 20 m model with bed level at corners (20 m cor), and finally the bed level at cell-centres averaged from the corner values (20 m corcen). The approach to averaging the corner points to cell centres is expected to provide a good representation of the cross-sectional area compared to the hydrodynamic models.

Figure 4.10 shows that for the low discharge simulation of 50 m^3/s the water levels are similar for the three different models. For the bank-full discharge of 1300 m^3/s simulation, in Figure 4.11, the 20 m models are within –0.1 m to 0.3 m of the 40 m model and for the flood discharge of 3200 m^3/s simulation the 20 m models are within –0.1 m to 0.1 m of the 40 m model (see Figure 4.12).

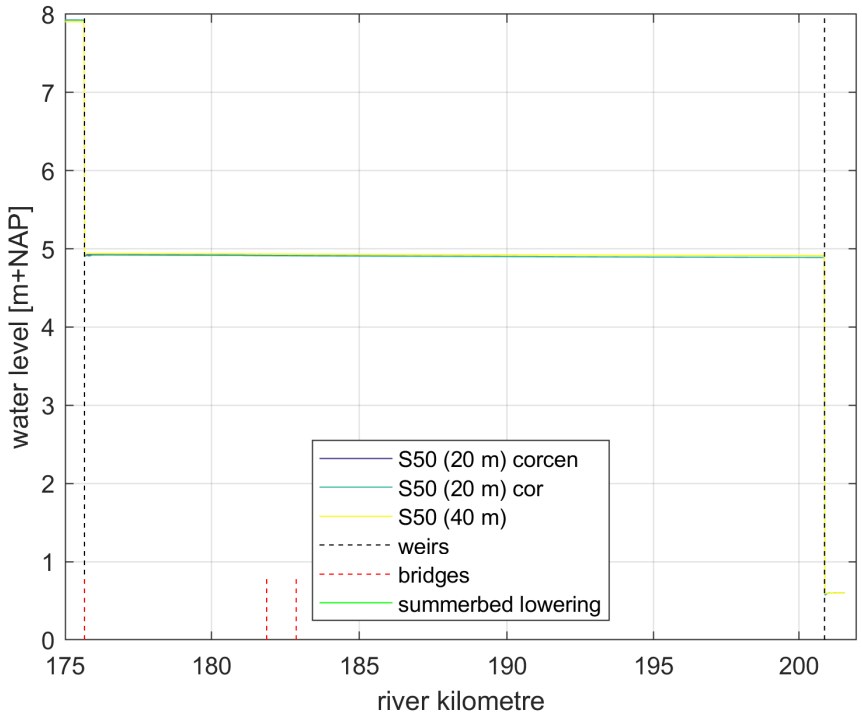

Figure 4.10 Water levels for the 50 m^3/s simulation from the 20 m corner model, 20 m corner to centre model, and the 40 m model.

In Figure 4.13, Figure 4.14, and Figure 4.15, the flow velocity magnitudes for the 20 m model are compared to the 40 m model. Here it can be seen that the flow velocities behave similarly to the 40m, but sometimes small differences are visible. For a discharge of 50 m^3/s, the difference between the weir at Grave and Lith is smaller than 0.05 m/s, for a discharge of 1300 m^3/s the difference is smaller than 0.15 m/s and for a discharge of 3200 m^3/s the difference is smaller than 0.10 m/s.

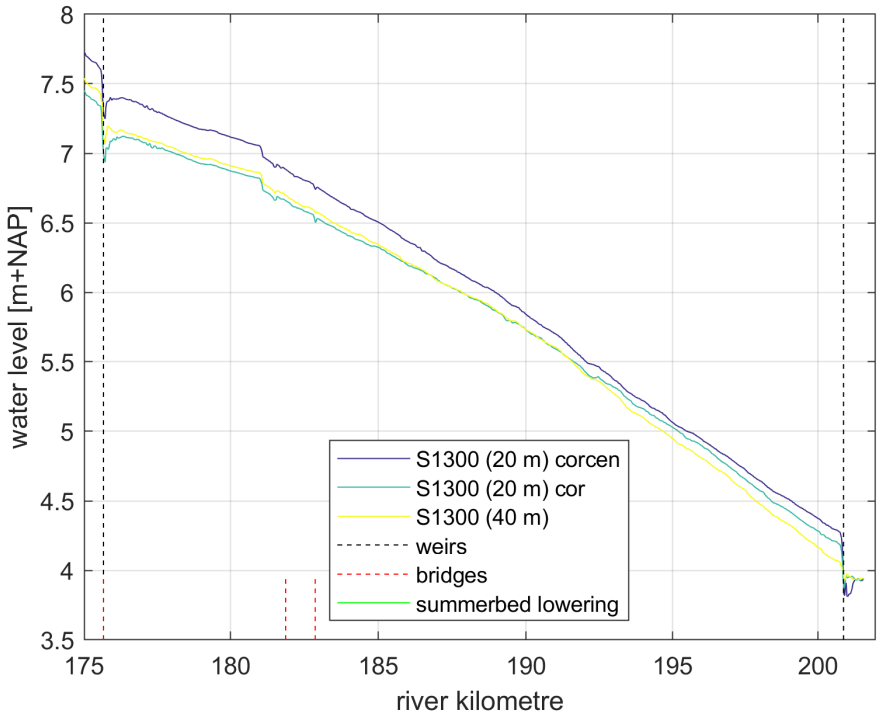

Figure 4.11 Water levels for the 1300 m^3/s simulation from the 20 m corner model, 20 m corner to centre model, and the 40 m model.

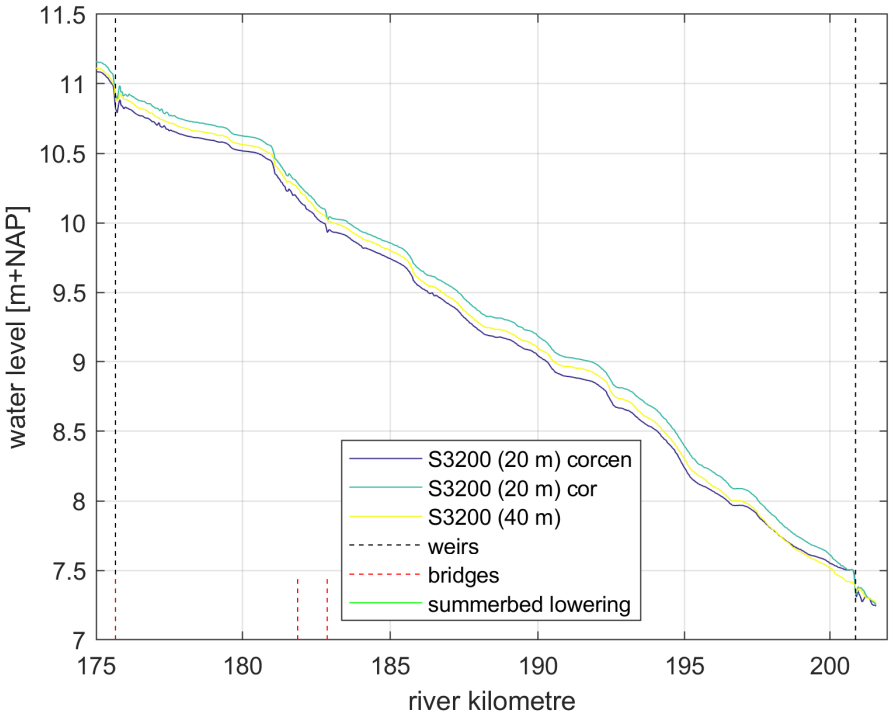

Figure 4.12 Water levels for the 2100 m^3/s simulation from the 20 m corner model, 20 m corner to centre model, and the 40 m model.

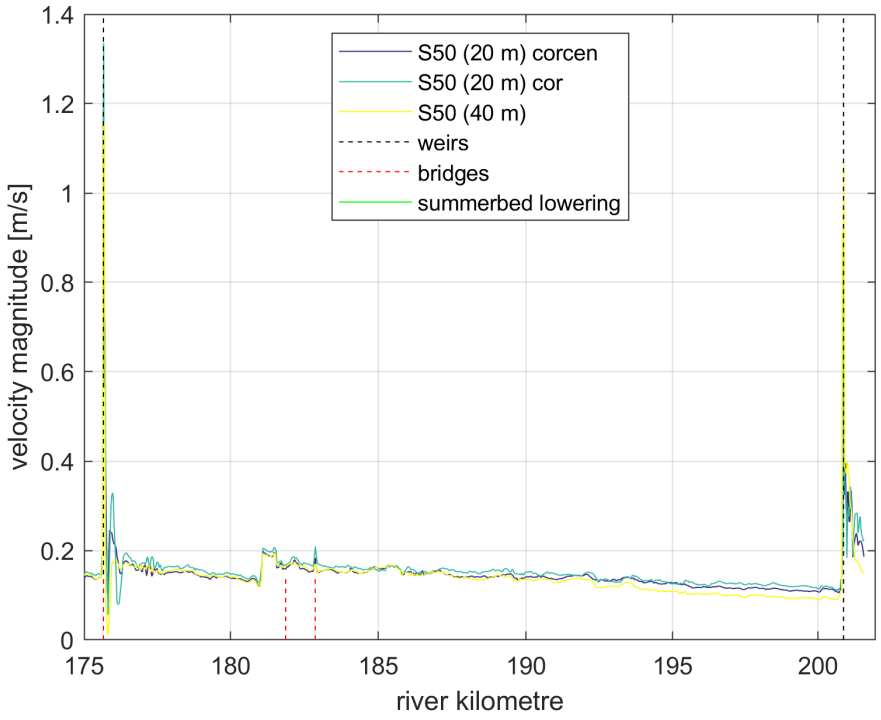

Figure 4.13 Velocity magnitude for the 50 m^3/s simulation from the 20 m corner model, 20 m corner to centre model, and the 40 m model.

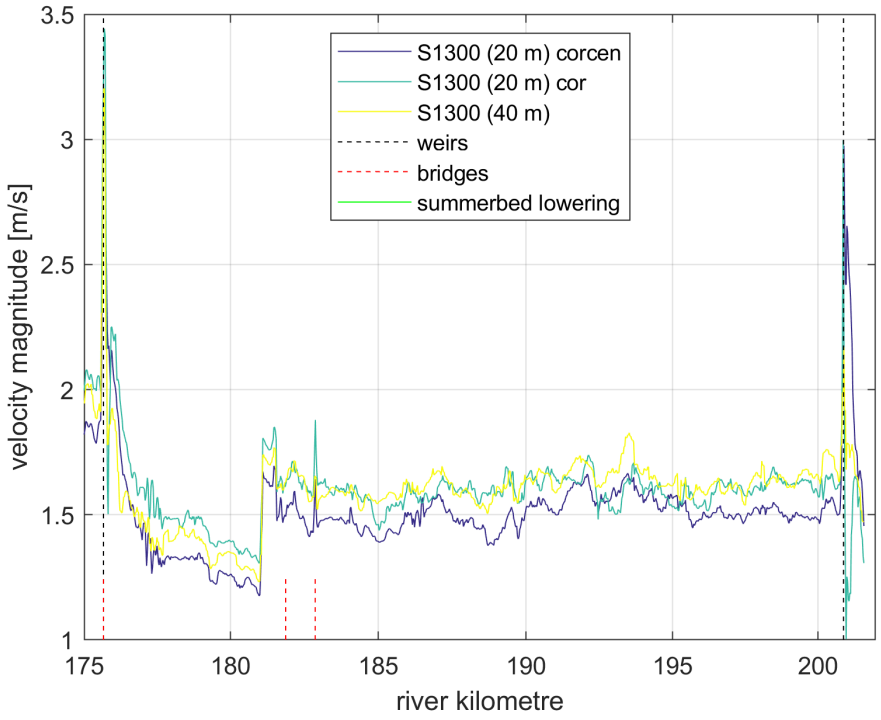

Figure 4.14 Velocity magnitude for the 1300 m^3/s simulation from the 20 m corner model, 20 m corner to centre model, and the 40 m model.

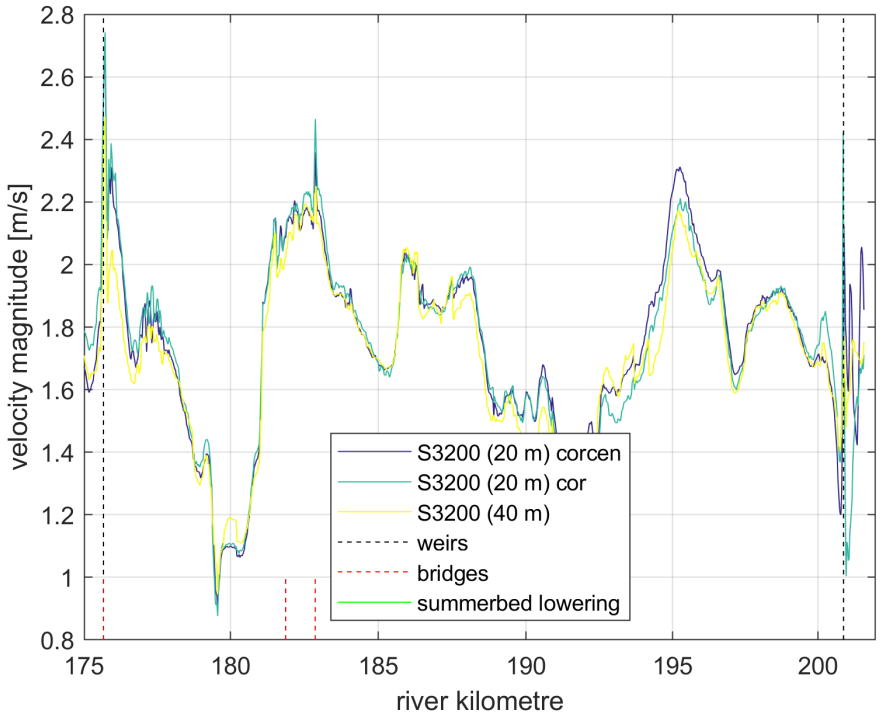

Figure 4.15 Velocity magnitude for the 3200 m^3/s simulation from the 20 m corner model, 20 m corner to centre model, and the 40 m model.

4.5 Calibration of Chézy coefficient

In Figure 4.16 the roughness of the 40 m model is shown. For the low discharges (up to 750 m^3/s) this shows a small increase in roughness after rkm 190, while for the high discharges (above 750 m^3/s) the roughness decreases at these locations. Both at the location of the bridges at Ravenstein, rkm 182, and rkm 193 small jumps are visible in the roughness.

The roughness is prescribed using a Nikuradse roughness height computed as the simplified Van Rijn approach:

$$k = Ah^{0.3}\left[1 - e^{-Bh^{-0.3}}\right], \tag{4.1}$$

where h denotes the local water depth, and the constants $A = 0.1$ and $B = 2.5$ are defined as in the hydrodynamic model. In addition a calibration factor is applied to the main channel roughness.

For the morphodynamic simulations, the choice has been made to use a constant Chézy coefficient without a calibration factor, as the computed sediment transport directly relates to the main channel velocity. This choice is made by running hydrodynamic simulations for a discharge of 50, 1300 and 3200 m^3/s for the reach Grave to Lith, with different constant values for the Chézy coefficients and comparing this with the situation where the roughness differs within the reach. This can be seen in Figures 4.17, 4.18 and 4.19.

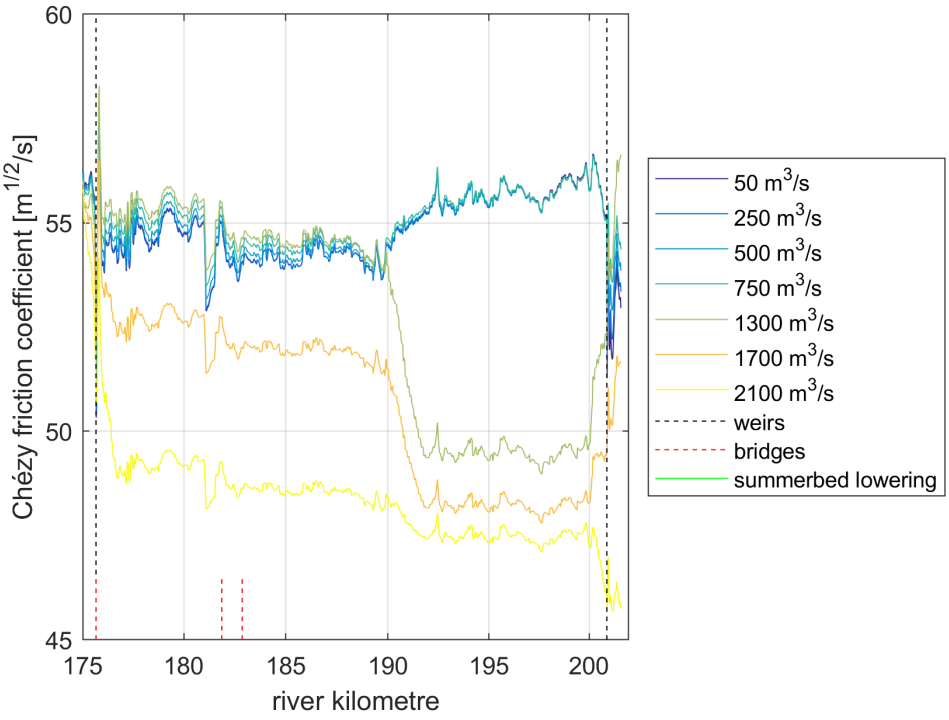

Figure 4.16 Width-averaged roughness for different discharges (L1R1).

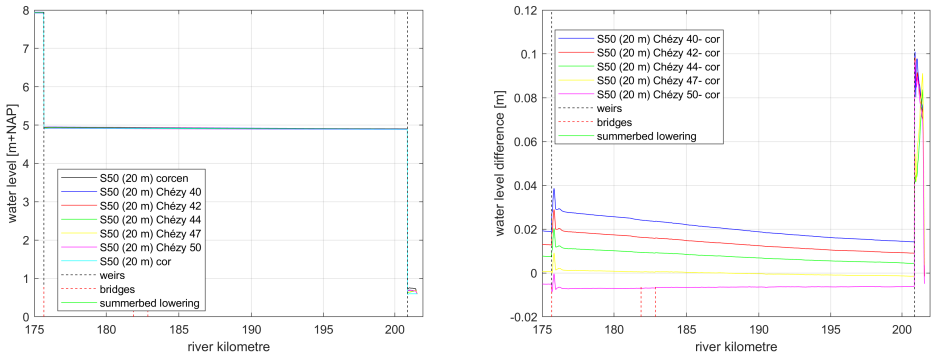

(a) (b)

Figure 4.17 Absolute water level (a) and water level difference (b) along the river axis for different values for different Chézy coefficients for a stationary discharge of 50 m^3/s.

In these figures it is visible that for a stationary discharge of 50 m^3/s, differences of up to 0.1 m can occur for the different Chézy values compared to the compared to the simulation with varying roughness in the reach. The highest differences occur near the weir. Looking at the reach between the weirs, the smallest differences occur for a constant Chézy coefficient of 47 $m^{1/2}/s$. For a discharge of 1300 m^3/s it can be seen that for a Chézy coefficient of 47 $m^{1/2}/s$ the water level gets overestimated upto 0.2 m, whereas for 50 $m^{1/2}/s$ the water level gets underestimated up to 0.15 m occur. This difference is higher, for the other values for the Chézy coefficients. Looking at a discharge of 3200 m^3/s, it can be seen that for a Chezy coefficient of 47 $m^{1/2}/s$, now the discharge gets underestimated up to 0.18 m.

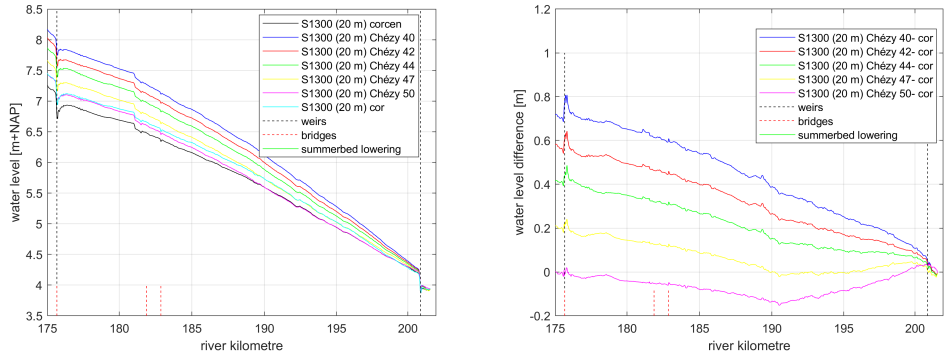

(a) (b)

Figure 4.18 Absolute water level (a) and water level difference (b) along the river axis for different values for different Chézy coefficients for a stationary discharge of 1300 m^3/s.

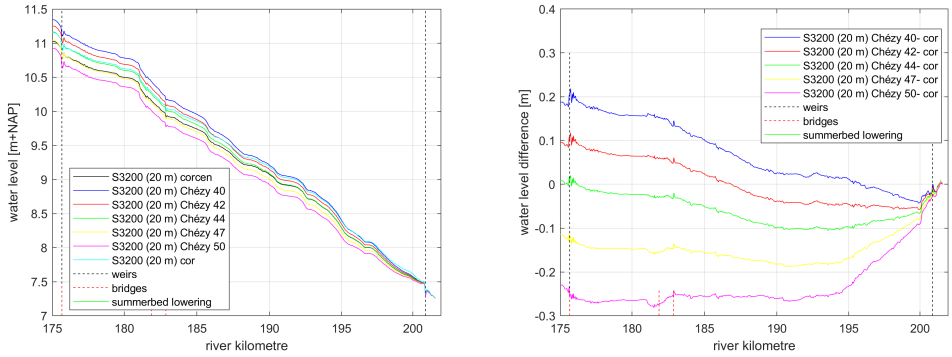

(a) (b)

Figure 4.19 Absolute water level (a) and water level difference (b) along the river axis for different values for different Chézy coefficients for a stationary discharge of 3200 m^3/s.

On average, a Chézy coefficient of 47 $m^{1/2}/s$ gives the best results compared to the simulation with varying roughness in the reach. This means that for the morphodynamic simulations this is used as the roughness value for the stretch between Grave and Lith.

4.6 Hydrodynamic spin-up

To save time, it is desirable to not need a new hydrodynamic spin-up for each new discharge level in the morphodynamic simulations. Therefore, a hydrodynamic spin-up database is created, where for each discharge level in the hydrograph, this discharge is simulated until the water level and discharge are stable. The end state of this simulation is then used as the hydrodynamic starting state in the morphodynamic simulation.

To ensure the simulation is stable, it needs to be checked whether the discharge and the water level is stable in the model domain. Since the upstream boundary is a discharge boundary it is most interesting to look at the velocity magnitude at the other end of the model domain, so near the downstream boundary. With the same reasoning, it is most interesting to look at the water level near the upstream boundary. This gives a good indication whether the water level and velocities are stable along the model domain.

All discharge levels have been simulated until the water level and velocities are stable. This means that the simulation duration for each discharge level is different. The water level at an upstream location and the velocities at a downstream location can be seen in Figure 4.20. For all simulations the water levels only show small differences of around 1 cm or less, while for the velocity magnitude all discharge levels are stable, except for a discharge of 3200 m^3/s. Here the velocity magnitude remains oscillating, but the difference is less than 2 cm/s. Therefore, this is deemed a good hydrodynamic starting point for the morphodynamic simulations.

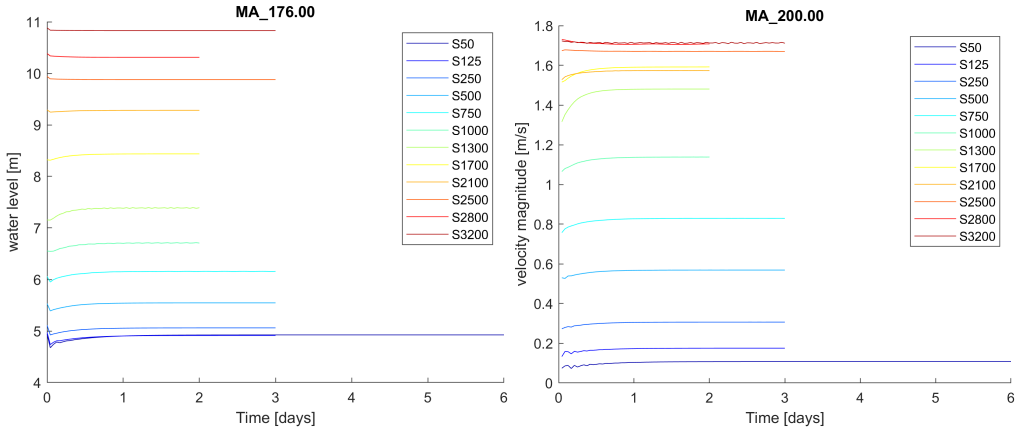

(a) (b)

Figure 4.20 Water levels near the upstream boundary (a) and velocity magnitudes near the downstream boundary (b) for each discharge level during the hydrodynamic spinup simulations.

5 Morphodynamic calibration

The current chapter focusses on the morphodynamic calibration of the Meuse sub-model between Grave and Lith. Before starting the calibration, the observed bed level changes are discussed. The calibration follows the following approach. Firstly, an order of magnitude of the sediment transport is evaluated by computing the offline sediment transport over a fixed bed. Sediment transport is evaluated for different combinations of parameters in the transport formula (Section 5.3). This leads to different combinations of parameters in the transport, which are evaluated in morphodynamic simulations (Section 5.4).

5.1 Observed trends between 2011 and 2021

Figure 5.1 shows the observed bed level development in the reach between Grave and Lith. As can be seen, between 2011 and 2020 there are some changes in bed level, but the most significant changes in bed level occur in 2021, the year of the flood event.

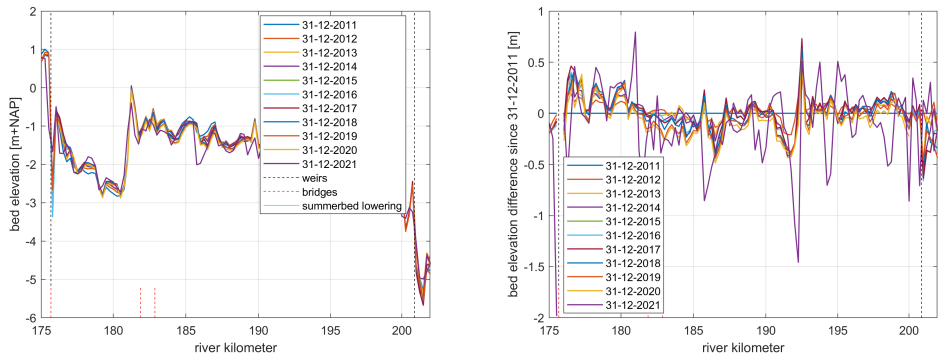

(a) (b)

Figure 5.1 Absolute bed level (a) and bed level difference (b) along the river axis between 31 December 2011 and 31 December 2021, based on measurements

The data presented in Figure 5.1 concerns all data of a particular year. As we intend to include the flood wave of 2021 as a calibration sequence, we looked deeper into the measured data, to see if the precise measurement times are available.

Upon inspection of the recent data (2020-2022) between Grave and Lith four measurement sets were present, which appeared to all be measured on a single day. The days in which these were measured were: 17-01-2020, 15-03-2021, 05-08-2021 (see Figure 5.2) and 30-06-2022 (see Figure 5.3). The last data clearly shows that dredging has taken place, especially in the inner bends. This is a drawback compared to considering all the data in a certain year, without having dredging information. It is recommended to do a measurement prior to and after any dredging activity, and to take note of the dredging volumes per section.

Similar to the method in (Meijer, 2020a,b), the bed level measurements were averaged to the L3R3 polygons. The results of the averaging operation are shown in Figure 5.4.

Figure 5.2 Bed level measurement of 05-08-2021

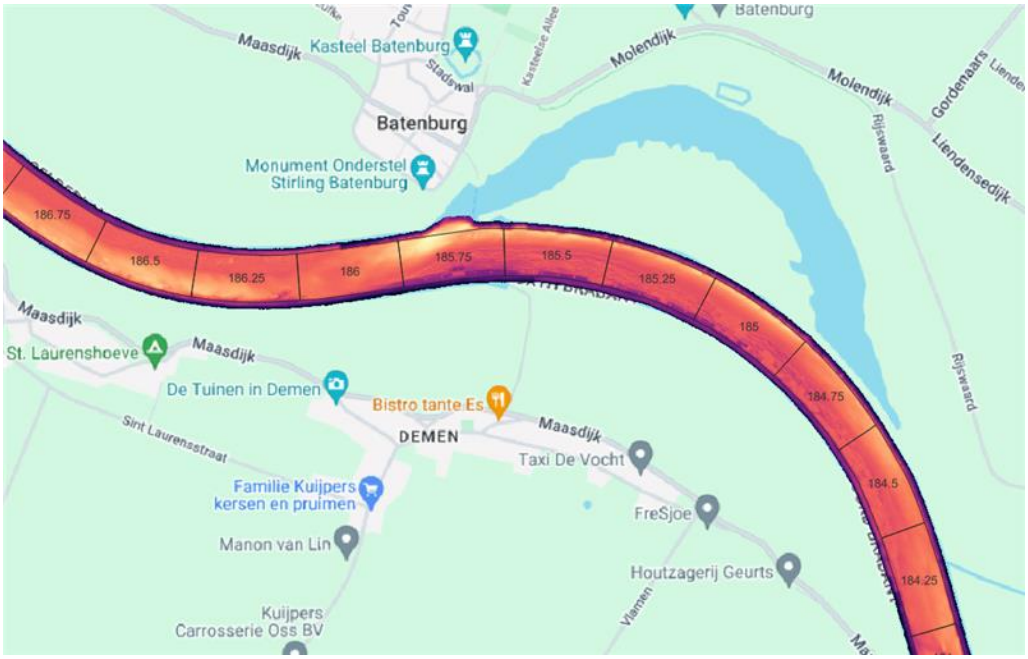

Figure 5.3 Bed level measurement of 30-06-2022

Considering the last data set in 2022 is clearly influenced by dredging activity, this data forms a trend break, and is not suitable for use in the hindcast for the current computations. For the remainder of the report, we limit our analysis to the period between 2011 and the measurement right after the flood wave of July 2021 (05-08-2021).

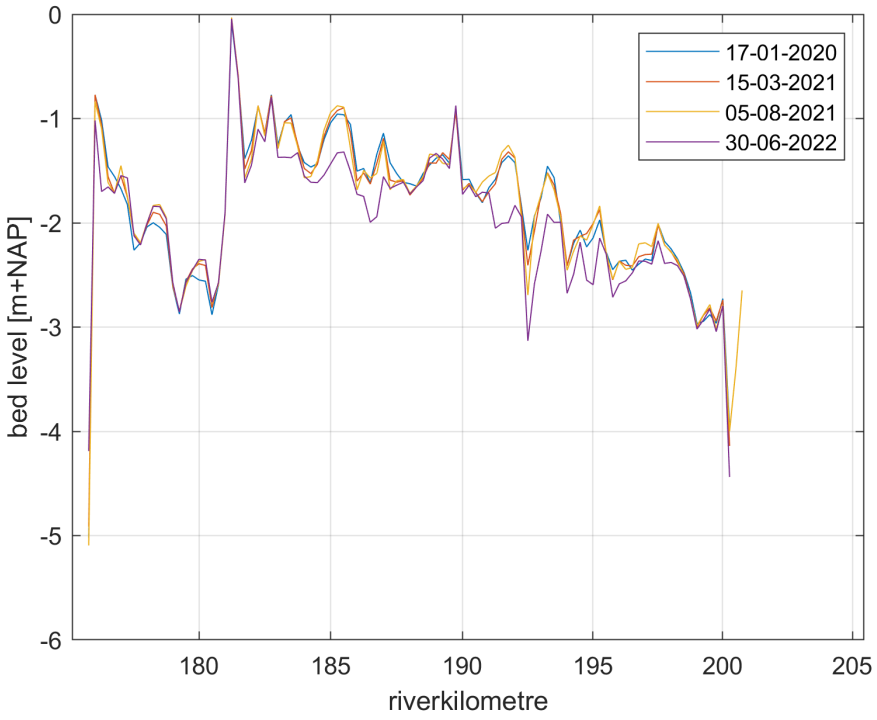

Figure 5.4 Bed level measurement averaged to L3R3 polygons along the Grave-Lith reach.

5.2 Estimation of the sediment transport

Using the bed level change averaged in the L3R3 polygons, we perform an integration of the bed level change between 31-12-2011 and 05-08-2021. By integrating the bed level change of the area, we can derive a lower bound of the sediment transport, up to a integration constant (see Figure 5.5). The graph shows an oscillating trend along the river reach. A jump of approximately 10 000 m^3 (including pores) is found from rkm 176 to 181. This value is used as an objective for the offline transport calibration in Section 5.3.

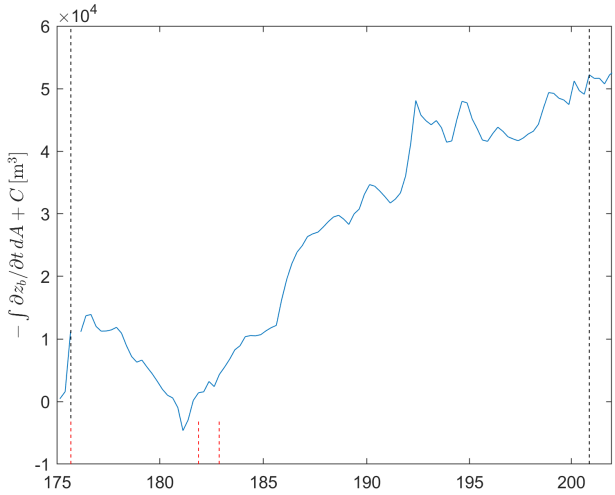

Figure 5.5 Lower bound of the transported volume of sediment between 31-12-2011 and 05-08-2021 in the reach Grave-Lith using the averaged bed level to L3R3 polygons, up to a integration constant.

.

5.3 Offline calibration

For the calibration of the morphological simulation it is necessary to determine the sediment transport relation. As a starting point the sediment transport relation of Meyer-Peter and Müller (1948) including a hiding-exposure correction by Parker *et al.* (1982) as we consider that this sediment transport formula should reasonably reproduce the graded sediment transport in the river Meuse.

To determine the sediment transport, Figure 5.6 shows the minimum sediment transport over the reach and the sediment transport including pores for different values of the multiplication factor A_{cal} and varying hiding exposure component β.

The increase in sediment transport around 182 km is caused by the jump in the bed shear stress as visible in Figure 6.7 and the decrease of sediment transport after rkm 195 is caused by drop in the bed shear stress for the high discharges 1700 m^3/s and 2100 m^3/s.

Using the transport estimate of 5.2, one can evaluate different options of A_{cal} and the hiding exposure exponent β (A_{SKLHE}) by the formulation of Parker *et al.* (1982). Evaluating these options leads to an estimated transport for the period between 31-12-2011 and 05-08-2021 (c.f. Figure 5.7). This provides an estimate for the morphodynamic changes, namely A_{cal}=0.125 and β=0. This is a low value compared to the standard A_{cal}=8 for the Meyer-Peter and Müller-formula.

Unfortunately, because of a typing error in the processing script the transport of 100 000 m^3 was evaluated, rather than 10 000 m^3 (`10e4` rather than `1e4`) as determined from the integrated bed level changes in 5.5. This line is also displayed in Figure 5.7. This lead to an estimate of A_{cal}=1.25 and A_{SKLHE}=0, which was also used in the morphodynamic simulation in Section 5.4. As the simulations are done, this cannot be changed at present, but is left to be tested for the next simulation.

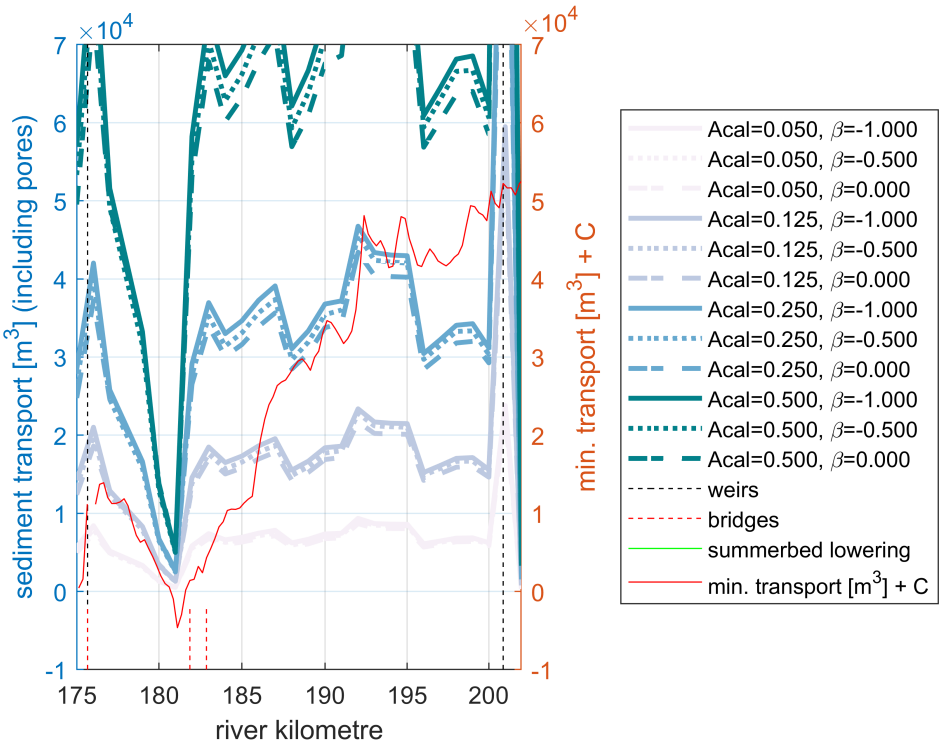

Figure 5.6 Evaluation of the sediment transport for varying multiplication factor A_{cal} and hiding exposure exponent β (left axis), versus a estimate of the minimum sediment transport based on bed level changes (right axis).

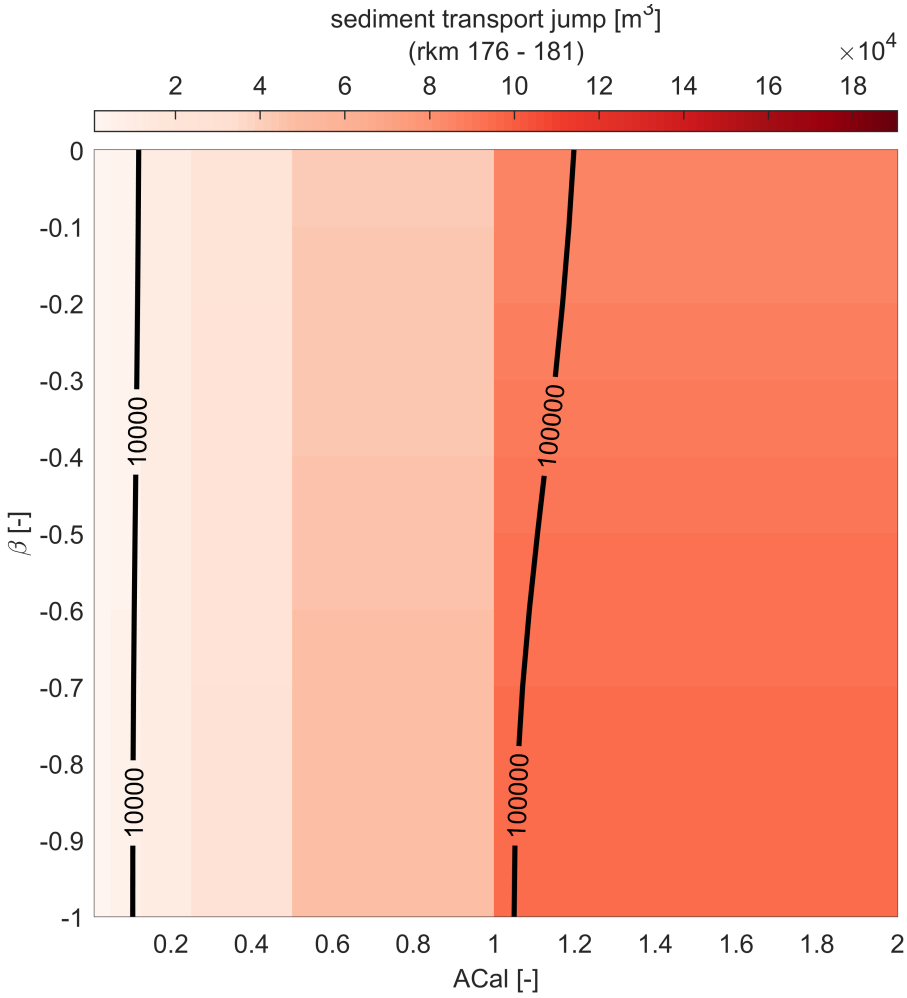

Figure 5.7 Computed transport with variation of multiplication factor and hiding exposure exponent. The black lines indicate a jump in the transport between rkm 176 and 181 of 10 000 m^3 and 100 000 m^3.

5.4 Simulations with morphological change

Using the information from Section 5.2, the following simulation is set up (see Table 5.1). It uses the general formula written as the standard Meyer-Peter and Müller (1948) formula, with a lower calibration factor of the transport A_{cal}=1.25 and not considering hiding and exposure (β=0, Parker *et al.* (1982)).

Table 5.1 Simulation with morphological change.

Simulation	A_{cal}	Hiding-exposure A_{SKLHE}	(θ_{cr})
MPM without hiding	1.25	β = 0	0.047

To reduce the influence of the weir zones from the computation, some zones have been added to the simulation, where the transport is computed, but it does not contribute to the bed level change using the keyword `MorphoPol`. This is applied upstream of rkm 175.95 and downstream of rkm 200.5.

6 Results

6.1 Fixed bed hydrodynamics

The simulation management tool runs sequential steady state simulations with a constant discharge. This enables the use of discharge-dependent inputs and parameters such as morphological factors, which help to reduce the simulation time Yossef *et al.* (2008). In the following figures, the hydraulic parameters are presented to gain insight into the different parameters at different discharges.

The hydraulic parameters which are investigated are the water level, water depth, depth-averaged velocity, discharge distribution and bed-shear stress.

Figure 6.1 shows the water level for different discharges along the reach. For low discharges the water level remains fairly constant, while for the higher discharges the negative gradient in the water level along the reach increases.

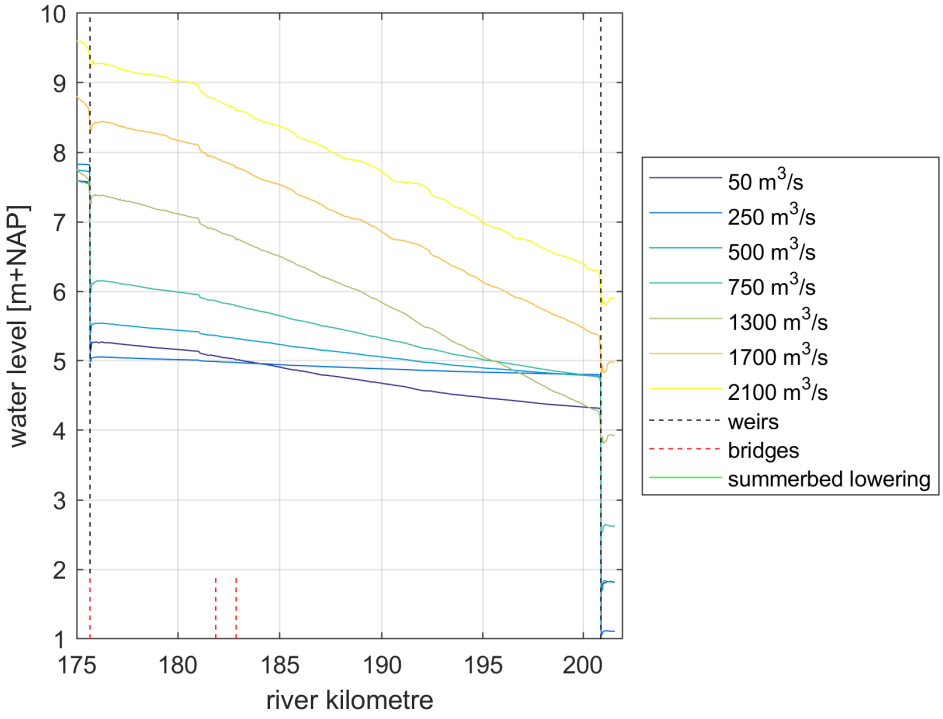

Figure 6.1 Width-averaged water levels for different discharges.

The water depth is shown in Figure 6.2. It shows shallow regions near the weir at Grave. Between rkm 176 and 181 a deeper zone is visible, which corresponds to the main-channel bed-level lowering. Around rkm 182 a shallow region is visible near the bridges at Ravenstein. The water depth gradually increases towards the weir at Lith. At the weir at Lith a shallow zone is visible again.

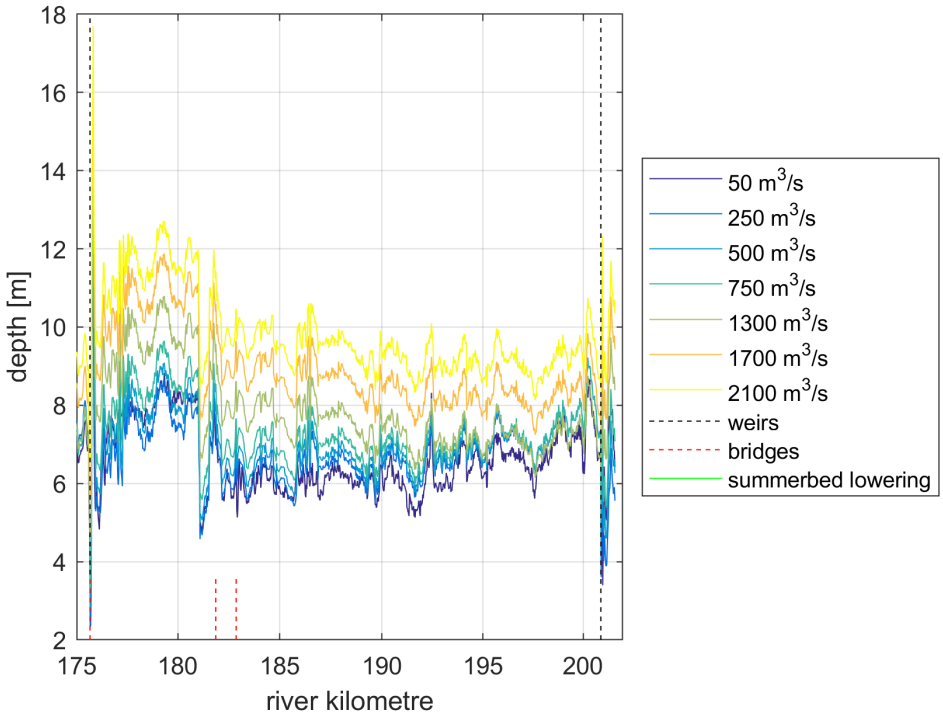

Figure 6.2 Width-averaged water depths for different discharges.

The velocity magnitude along the river axis is shown in Figure 6.3. For all discharges a slightly negative gradient is visible along the reach. Between rkm 176 and 181 a slightly lower average velocity is found compared to the the reach average. Around the bridges at Ravenstein, rkm 182, the velocity increases due to the shallow region there. For the highest discharges (1700 m^3/s and 2100 m^3/s) there is an oscillating pattern in the flow compared to the 1300 m^3/s discharge, which is likely caused by the flow to and from the main channel. For the largest discharge, the lowest velocities on the river axis occur at rkm 185, 189, 192, 197 and the highest velocities occur at 182, 186, 191, 195.

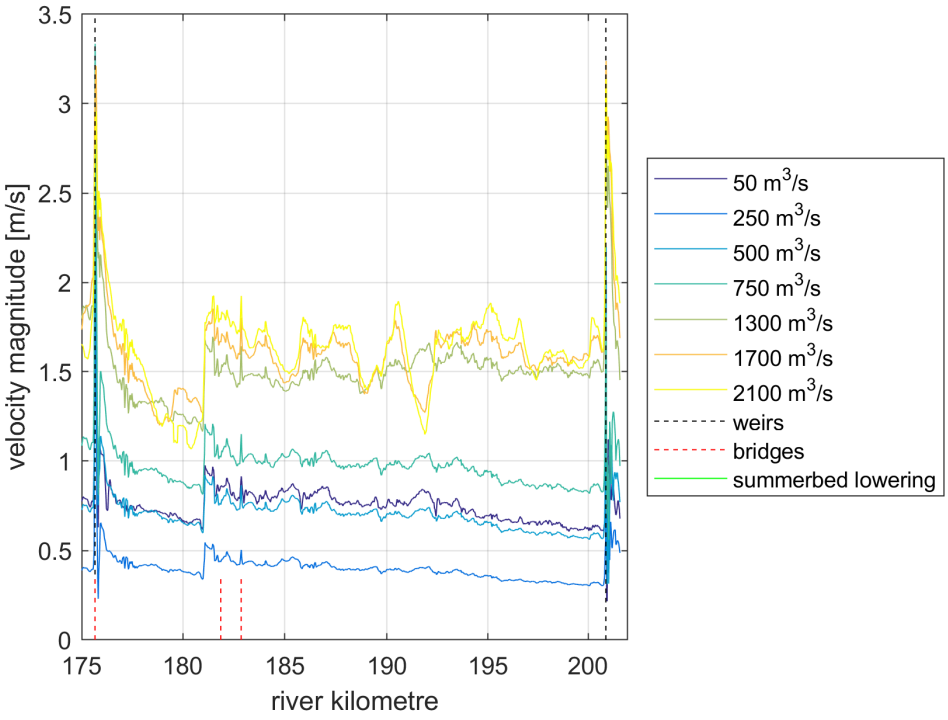

Figure 6.3 Width-averaged velocity magnitude for different discharges (L1R1).

Using the hydrodynamic simulations for the 20 m grid the discharge distribution is presented for the steady discharges 50 m^3/s, 1300 m^3/s and 2100 m^3/s in Figure 6.4, Figure 6.5 and Figure 6.6, respectively. The pattern for the discharges 50 m^3/s and 1300 m^3/s is fairly constant along the channel. For the discharge 2100 m^3/s, the flow exchange between the main channel and the floodplains is clearly visible.

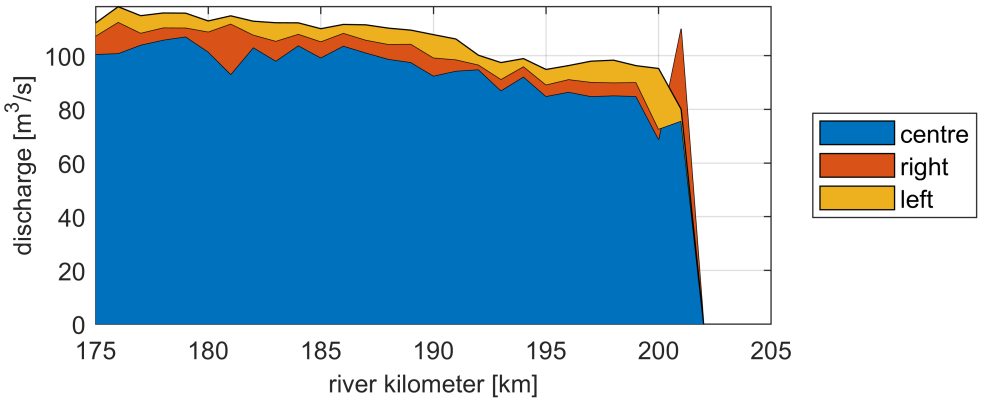

Figure 6.4 Discharge distribution in center (L3R3), left and right floodplains for steady discharge of 50 m^3/s.

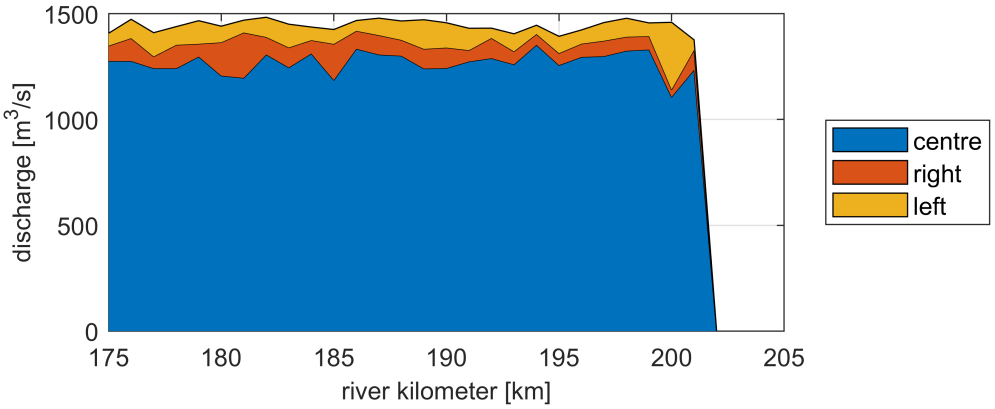

Figure 6.5 Discharge distribution in center (L3R3), left and right floodplains for steady discharge of 1300 m^3/s.

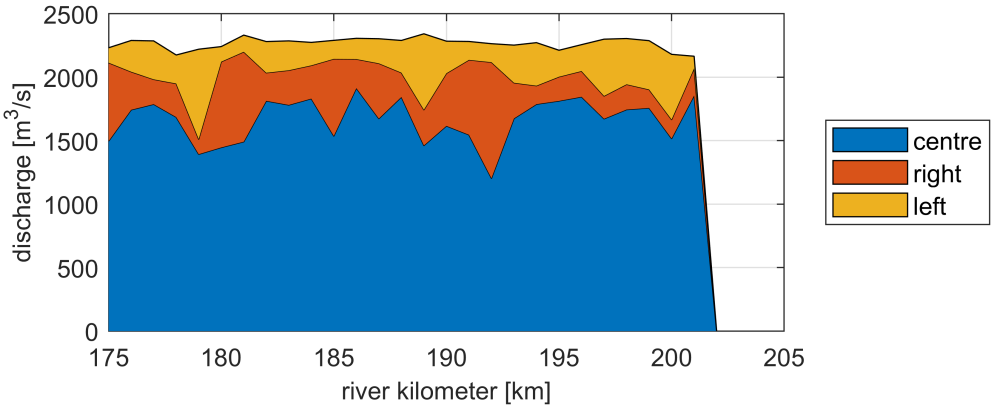

Figure 6.6 Discharge distribution in center (L3R3), left and right floodplains for steady discharge of 2100 m^3/s.

The resulting bed shear stress per discharge level is shown in Figure 6.7. The bed shear stress largely follows the pattern in the velocity and gradually decreases until Ravenstein, where a sudden jump occurs in bed shear stress. After the bridges the bed shear stress remains fairly constant, except for the peak caused by the lower bed level near rkm 193. Again the largest discharges show an oscillating pattern.

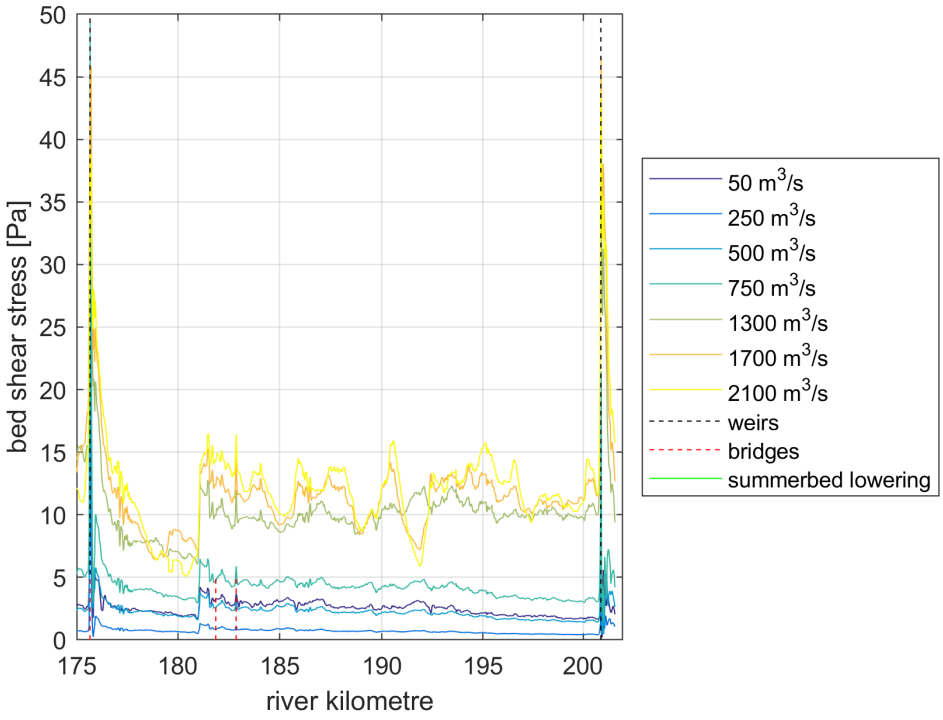

Figure 6.7 Width-averaged bed shear stress for different discharges (L1R1).

6.2 Bed level development

The initial bed level in the simulations is shown in Figure 6.8. There is some difference in the simulation bed level versus the measured bed level, and this can be attributed to the method in which the bed level was interpolated from the multibeam measurements. A more time-consuming approach which should give comparable results is to perform a grid cell averaging operation directly on the multibeam data. In the current simulations the bed level in the main channel was imposed by a nearest neighbour interpolation from the measured multibeam data (cf. Section 3.4). This is left as a recommendation for further interpolations.

Figure 6.9 shows the absolute bed level after almost 10 years of computation and from measurements. The bed level changes with respect to 31-12-2011 are shown in Figure 6.10.

On the reach scale, the bed level development after 10 years of development agrees well between the model and measurements. The overall bed slope in the reach (rkm 183-200) is well reproduced.

Locally, some differences exist. For example, at the upstream boundary local erosion occurs, which may be related to the incorrect incoming sediment. There appears to be too much sedimentation in the main-channel bed-level lowering at rkm 176. In addition, downstream of the Niftrik fixed layer 181-181.5 the model predicts too strong erosion. Locally, at rkm 186, 192 and 194, erosion occurs in the measurements which is not captured by the computation.

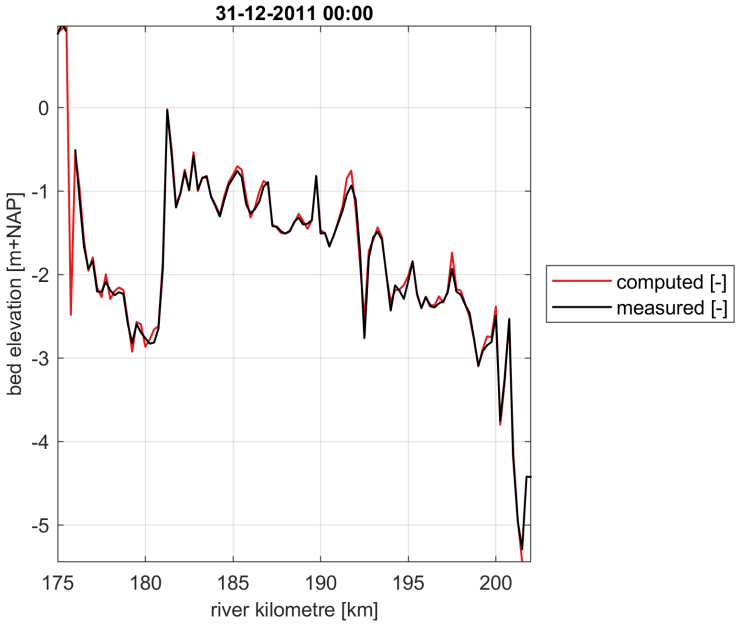

Figure 6.8 Initial bed level in the models and from measurements at 31-12-2011

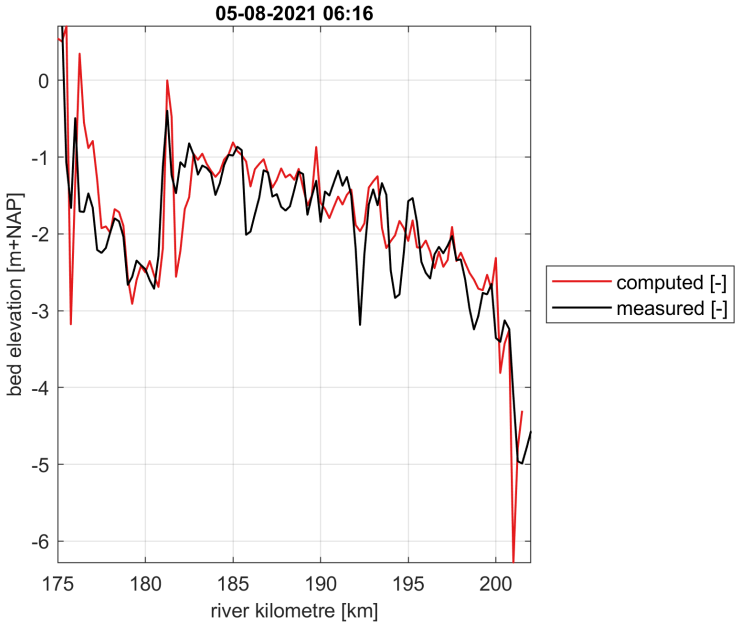

Figure 6.9 Final bed level in the simulations and from measurements at 05-08-2021

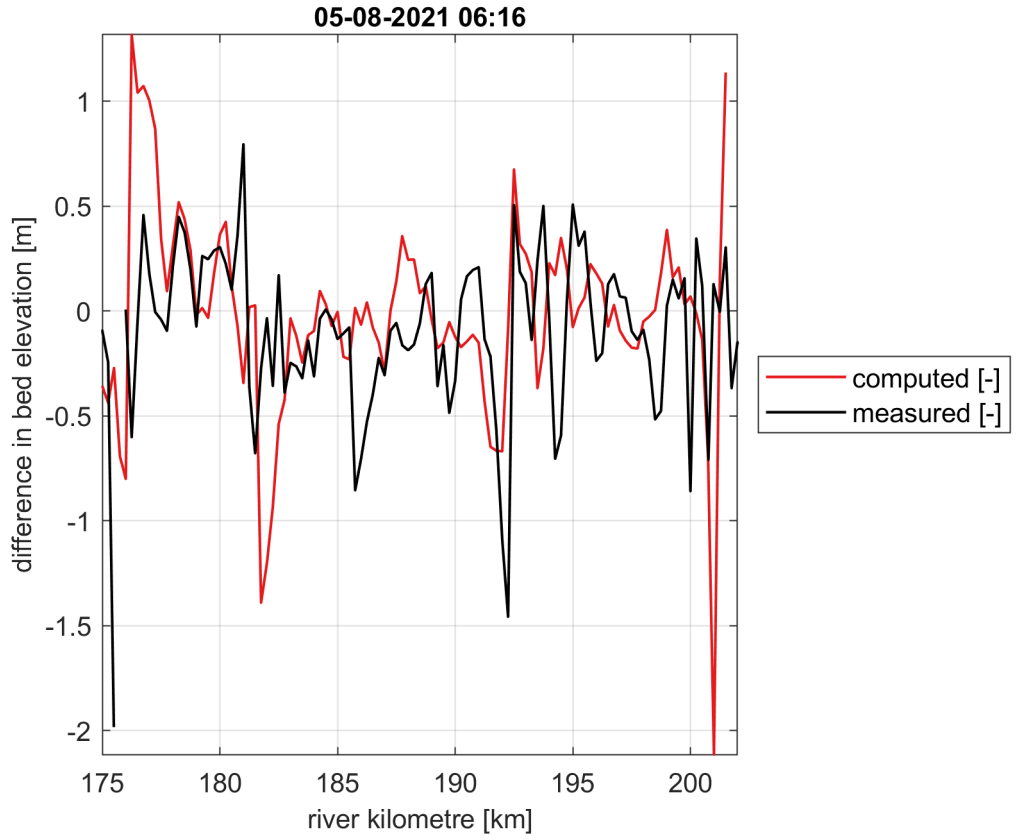

Figure 6.10 Bed level change w.r.t. 31-12-2011 at 05-08-2021

7 Discussion

The report showed that it was possible to perform a reasonable conversion of the 40 m to a shorter 20 m grid model for the stretch between Grave and Lith. An important contribution is the setting of the weir levels, to avoid the coupling to D-RTC. In addition, the initial fields are also translated from the coarse to the fine grid. This method is extendable to other reaches, based on the already completed simulations for the 40 m grid.

It was found that in the 20 m grid model the sluices near the weirs are not closed off after projection of the fixed weirs. This lead to strong flow through the sluice at Lith for low to medium discharges. It is therefore left as a recommendation to include the sluices and other potential leaks to the Baseline schematisation.

An improved procedure for the definition of sediment availability was added, which allows the addition of new fixed zones in the future. Currently, the sediment availability was limited to the L3R3 polygons and set to zero thickness where fixed layers are present.

Careful inspection of the received multi-beam data was needed, as dredging was clearly apparent in some of the measurements. Without a dredging criterium in place it is not possible to use this measurement for a hindcast simulation. It is recommended to perform a multi-beam measurement prior to and after the dredging activities. In addition, the availability of measurements covering a long connected reach, measured within a day, as was the case in the reach Grave-Lith, is very useful to understand the dynamics of the river bed.

Integrating the bed level changes along the channel leads to a considerably lower transport in comparison to the standard Meyer-Peter and Müller formula. Based on the jump in sediment transport across the main-channel bed-level lowering between 176 and 181 a first estimate of the sediment transport parameters was found. Unfortunately, due to a typing error the offline calibration lead to an overestimate of the jump, and possibly an overestimation of the computed transport.

The specific choice of the parameters of the transport formula (A_{cal}=1.25 and a hiding exposure exponent β=0), which appear to overestimate the transport (based on the minimal bed level changes), do lead to good agreement between the measured and modelled bed level development over the reach. The overall bed slope in the reach (rkm 183-200) is well reproduced, which indicates that the actual transport could in fact differ from the minimum offline sediment transport estimate.

The sedimentation at the upstream boundary and the too strong erosion downstream of the fixed layer at Niftrik, may be explained by the overestimation as determined from the offline transport calibration. To confirm or rule this out as a possibility, an additional simulation using smaller value of A_{cal}=0.125 is recommended.

Another option could be that the upstream boundary transport needs a reduction, as not all sediment is expected to pass the weir Grave which is located upstream.

Downstream of the fixed layer the sediment passing over could be too low. The correction of transport over fixed layers (Struiksma, 1985) may have a too strong influence at this location. It is recommended to look into the influence of an initial sediment thickness, and the parameter THRESH to see how the result is influenced by these parameters.

Locally, at rkm 186, 192 and 194, erosion occurs in the measurements which is not captured by the computation. It is recommended to investigate the bed level changes at these locations, to determine what is responsible for the erosion there. Subsequently, the model should be checked to see what could be adjusted to improve the local development.

It is known that the initial changes in a model could be due to the resolution of the numerical discretisation and the accuracy of the described physics. Using a certain spin-up period could be useful to help the model adapt to the initial differences caused by the numerical discretisation.

Furthermore, the analysis has been limited to a main channel averaged analysis of the trends. For the next phase it is recommended to consider the bed level development in the transverse direction as well.

8 Conclusions and recommendations

An initial morphological simulation for the reach Grave-Lith was setup using a 20 m grid, based on boundary conditions, initial fields and weir settings from the 40 m hydrodynamic model.

Simplification of the roughness lead to a constant roughness Chézy=47 $m^{1/2}/s$ which approximated the water levels in the 40 m hydrodynamic model.

The model has not undergone an elaborate calibration, but a good selection of the data and preparation of hydrodynamic simulations has been done. The offline analysis of transport has shown to be a good starting point for further simulations based on the bed level evolution, but requires a refined assessment, which may improve the initial one-dimensional result even further.

Calibration of the incoming sediment transport, and the influence of different parameters for the fixed layer are necessary to complete the one-dimensional calibration.

Including the comparison of two-dimensional effects (i.e. the development of the transverse bed level) is an important next step in the model calibration.

Furthermore, it is recommended to see how the result changes by considering a spin-up period, or a smoothing of the initial bed level and sediment composition. This is required to gain understanding of the adaptation of the model to the initial conditions.

Finally, when the two-dimensional calibration is completed, a comparison of the same discharge sequence 2011-2021 considering a measure in the floodplain like the Meanderende Maas would be good, to see if the model including a measure produces plausible results, compared to the model without the measure.

References

Becker, A., A. Kosters, A. Nunes de Alencar Osorio, V. Chavarrias and W. Ottevanger, 2023. *Morphological model for the river Rhine : First (v0) model of the Waal branch*. rapport Deltares, Deltares, Delft.

Berends, K., R. Daggenvoorde and K. Sloff, 2020. *Morphological models for IRM: Meuse 1D*. Tech. Rep. 11203684-015-ZWS-0016, Deltares and HKV.

Chavarrias, V., 2021. *Differences between parallel and sequential simulations*. Tech. rep., Deltares, the Netherlands. Presentation.

Chavarrias, V. and W. Ottevanger, 2022. *Modelling study of the sediment transport along the Meuse River during the flood wave of 2021*. Memo 11208012-013-ZWS-0001, Deltares, Delft, the Netherlands.

van der Deijl, E., 2023. *Validatie hoogwater Maas juli 2021*. rapport Deltares, Deltares, Delft.

van der Deijl, E. and W. Ottevanger, 2023. *Bodemschuifspanning Gemeenschappelijke Maas: Duiding op basis van modelberekeningen en veldmetingen*. Tech. rep., Deltares, Delft, the Netherlands.

Engelund, F. and E. Hansen, 1967. *Monograph on sediment transport in alluvial streams*. Tech. Rep., Hydraulics Laboratory, Technical University of Denmark, Copenhagen, Denmark.

Frings, R., 2022. *De bodemsamenstelling van de Maas in 1983 en 2020*. Tech. Rep. only data - report to follow, Rijkswaterstaat.

Fujisaki, A., R. Agtersloot and A. Becker, 2022. *B&O-modellen en deelmodellen Maas.* Tech. Rep. 11208053-002-ZWS-0005 v2.0, Deltares, Delft, the Netherlands.

Giri, S. and H. R. A. Jagers, 2022. *D-FAST Morphological Impact 2022: Part 2: Application in Case Studies and Testing of Algorithms*. rapport Deltares, Deltares, Delft.

Jagers, H. R. A. and S. Giri, 2022. *D-FAST Morphological Impact 2022: Part 1: Theory and Algorithms*. rapport Deltares, Deltares, Delft.

de Jong, J., 2021. *Ontwikkeling zesde-generatie Maas-model: Modelbouw, kalibratie en validatie*. Tech. Rep. 11200569-003-ZWS-0014, Deltares, Delft, the Netherlands.

Lely, C. W., 1926. *De Verbetering van de Maas voor Groote Afvoeren*. Tech. rep., Rijkswaterstaat.

Meijer, D. G., 2020a. *Kennis- en data-inventarisatie voor bodemhoogteanalyses Maas; Systeemrapportage morfologie Maas: Analyserapport (fase 2)*. Tech. Rep. 117.01-02, RiQuest.

Meijer, D. G., 2020b. *Kennis- en data-inventarisatie voor bodemhoogteanalyses Maas; Systeemrapportage morfologie Maas: Overzichtsrapport (fase 1)*. Tech. Rep. 117.01-02, RiQuest.

Meyer-Peter, E. and R. Müller, 1948. “Formulas for bed-load transport.” In *Proc. 2nd IAHR World Congress, 6–9 June, Stockholm, Sweden*, pages 39–64.

van der Mheen, M. and J. Prins, 2015. *Morfologische ontwikkelingen in de Grensmaas; Analyse van bodemveranderingen als gevolg van de Maaswerken met metingen en WAQMorf*. Tech. Rep. 1209376-000, Deltares, Delft, the Netherlands.

Mosselman, E., 2013. *Evaluatie WAQMorf*. Tech. Rep. 1205916-007, Deltares, Delft, the Netherlands.

Ottevanger, W., 2021. *Morphological model for the River Meuse: Case Study for the reach Sambeek-Grave*. Tech. Rep. 11206793-014-ZWS-0004, Deltares, Delft, the Netherlands.

Ottevanger, W., 2023. *D-Morphology: Implementation of a separate roughness field for morphodynamics*. Memo 11209261-002-ZWS-0002, Deltares, Delft, the Netherlands.

Ottevanger, W. and V. Chavarrias, 2022a. *Morphological model for the River Meuse: Case Study for the reach Lixhe-Keizersveer*. Tech. Rep. 11208033-002-ZWS-0005, Deltares, Delft, the Netherlands.

Ottevanger, W. and V. Chavarrias, 2022b. *Morphological model for the River Meuse: Case Study for the reach Sambeek-Grave*. Tech. Rep. 11208033-002-ZWS-0003, Deltares, Delft, the Netherlands.

Ottevanger, W. and V. Chavarrias, 2023. *Sedimenttransport Maas: Duiding op basis van literatuuronderzoek*. Tech. Rep. 11209470-002-ZWS-0001, Deltares, the Netherlands.

Ottevanger, W., V. Chavarrias, M. Busnelli, A. Omer and C. Eijsberg, 2024a. *Morphodynamic model of the Meuse River: Linne - Roermond v0.5, Roermond - Belfeld v0.5, Belfeld - Sambeek v0.5, Grave - Lith v0.5, Lith - Keizersveer v0.5*. Tech. Rep. 11210364-002-ZWS-0003, Deltares, the Netherlands.

Ottevanger, W., V. Chavarrias, S. Giri and E. van der Deijl, 2021. *Morphological model for the River Meuse: Model setup, input visualisation, and future steps*. Tech Rep. 11206792-003-ZWS-0002, Deltares, Delft, the Netherlands.

Ottevanger, W., V. Chavarrias and A. Omer, 2024b. *Morphological model for the River Meuse : Sambeek-Grave v0.8*. rapport Deltares, Deltares, Delft.

Ottevanger, W., E. Verschelling and S. Giri, 2020. *Initiële modelbouw morfologisch model voor de Maas*. Tech Rep. concept 11205234-003-ZWS-0001, Deltares, Delft, the Netherlands.

Parker, G., P. C. Klingeman and D. G. McLean, 1982. “Bedload and size distribution in paved gravel-bed streams.” *J. Hydraulics Div.* 108 (4): 544–571.

Rijkswaterstaat, 2023. *Rivierkundig Beoordelingskader voor ingrepen in de Grote Rivieren*. Tech. rep., Ministerie van Infrastructuur en Waterstaat, Rijkswaterstaat Water, Verkeer en Leefomgeving. (in Dutch).

Sieben, A., 2010. *Methodiek inschatting morfologische effecten in het zomerbed door lokale rivieringrepen*. Tech. Rep., Rijkswaterstaat.

Spruyt, A. and W. Ottevanger, 2019. *Plan van aanpak morfologisch model Maas*. rapport, Deltares, Delft.

Struiksma, N., 1985. *Celerity and deformation of bed perturbations travelling over a non-erodible layer*. Tech. Rep R657-48, W308, Delft Hydraulics Laboratory, Delft, the Netherlands.

de Vries, J. W., 1947. “De Maasverbetering voltooid.” *De Ingenieur* 32: 75–80.

Yossef, M. F. M., H. R. A. Jagers, S. van Vuren and A. Sieben, 2008. “Innovative techniques in modelling large-scale river morphology.” In M. Altinakar, M. A. Kokpinar, İsmail Aydin, Şevket Cokgor and S. Kirgoz, eds., *Procedings of the 4th International Conference on Fluvial Hydraulics (River Flow), 3-5 September, Cesme, Izmir, Turkey*. Kubaba Congress Department and Travel Services, Ankara, Turkey.

A Sediment availabilty

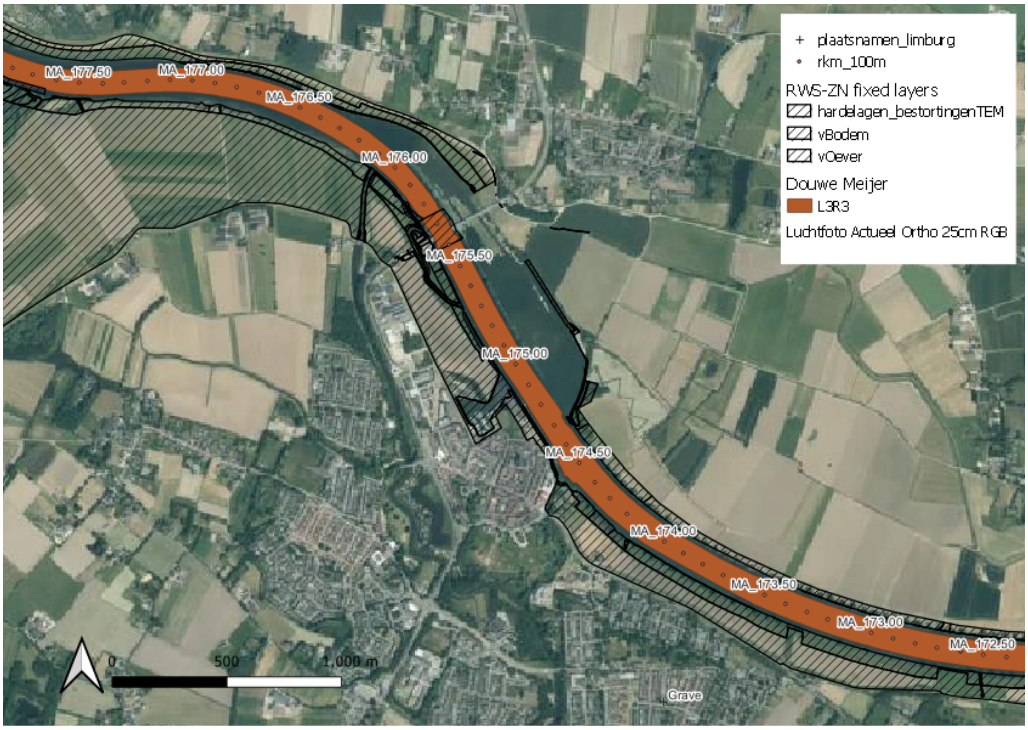

Figure A.1 Sediment availability in the Grave-Lith reach 1/11

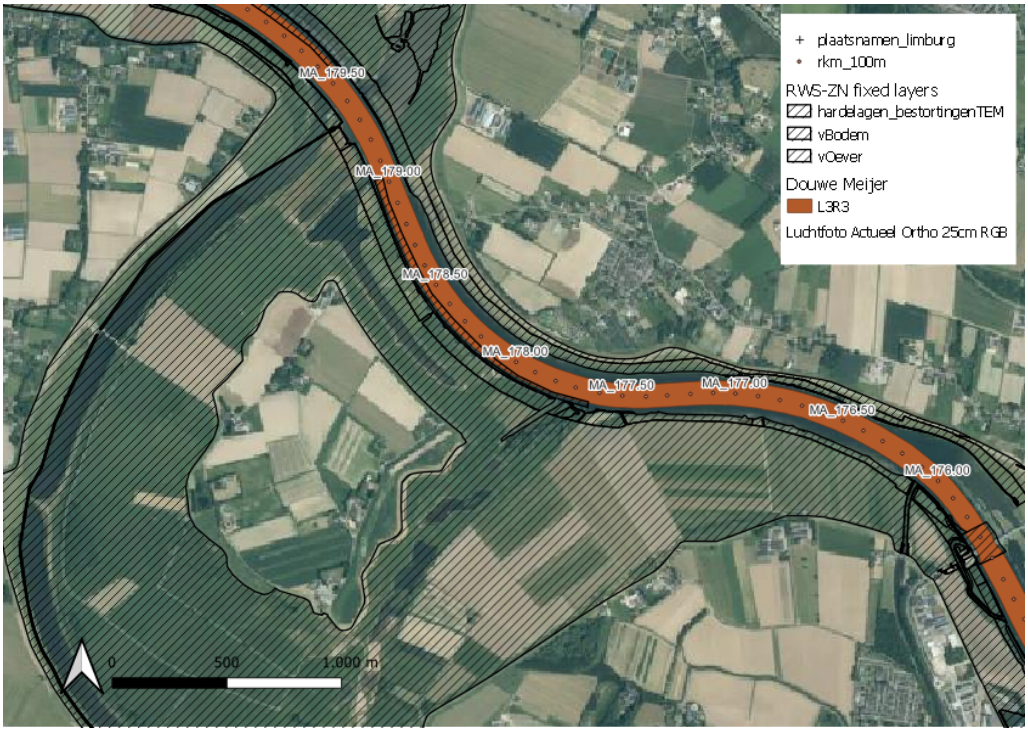

Figure A.2 Sediment availability in the Grave-Lith reach 2/11

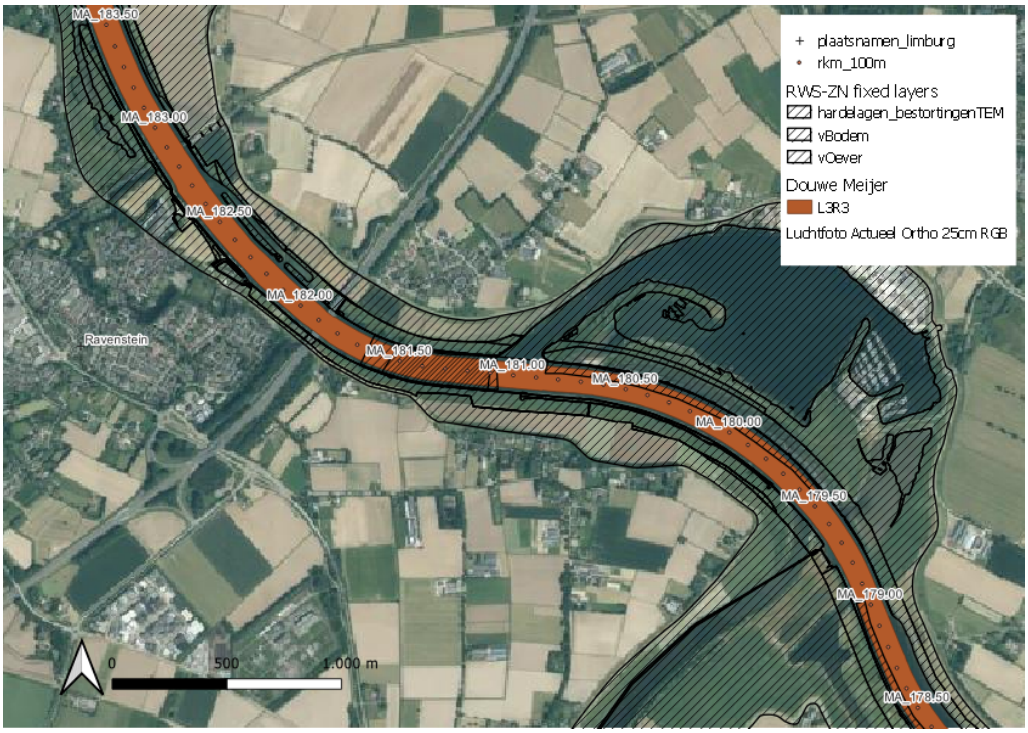

Figure A.3 Sediment availability in the Grave-Lith reach 3/11

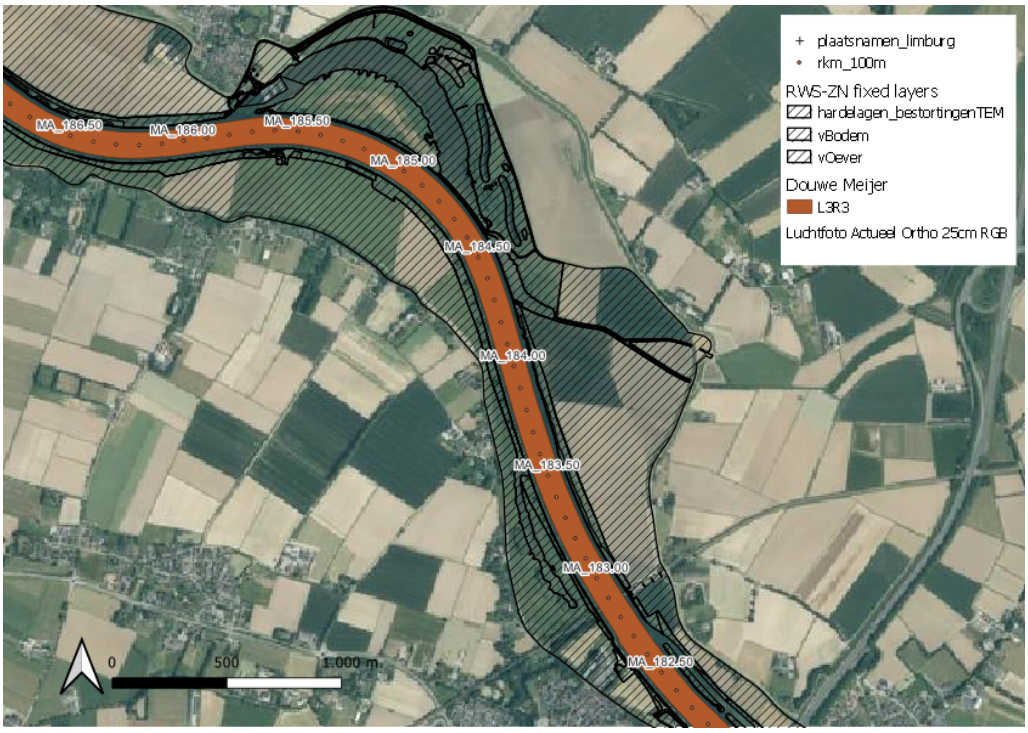

Figure A.4 Sediment availability in the Grave-Lith reach 4/11

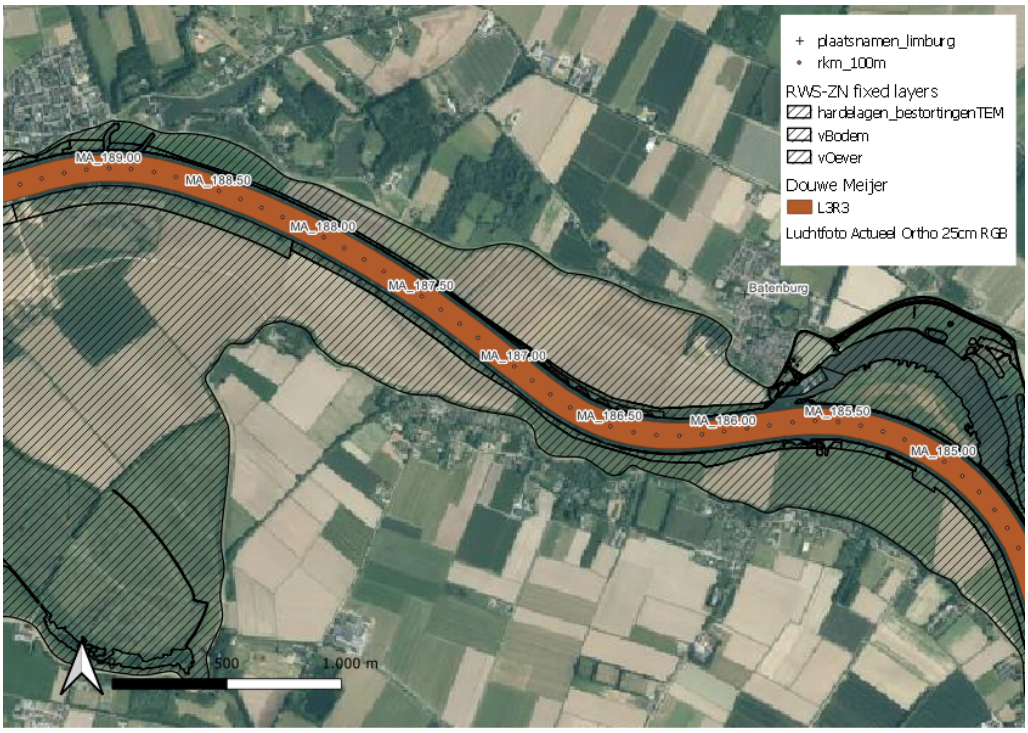

Figure A.5 Sediment availability in the Grave-Lith reach 5/11

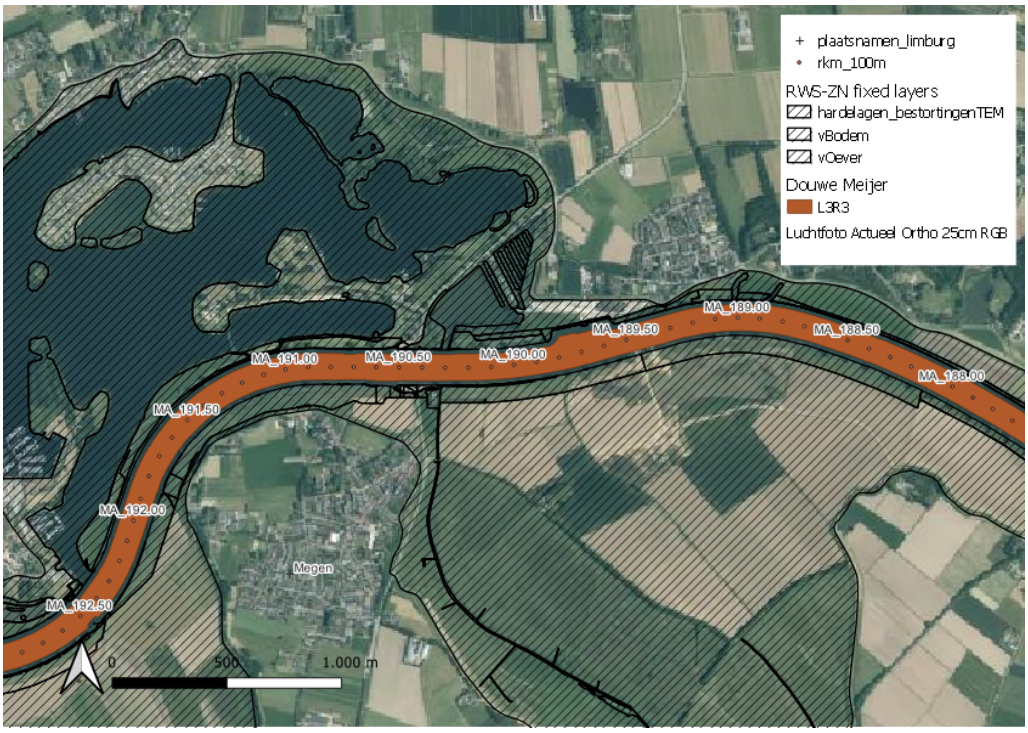

Figure A.6 Sediment availability in the Grave-Lith reach 6/11

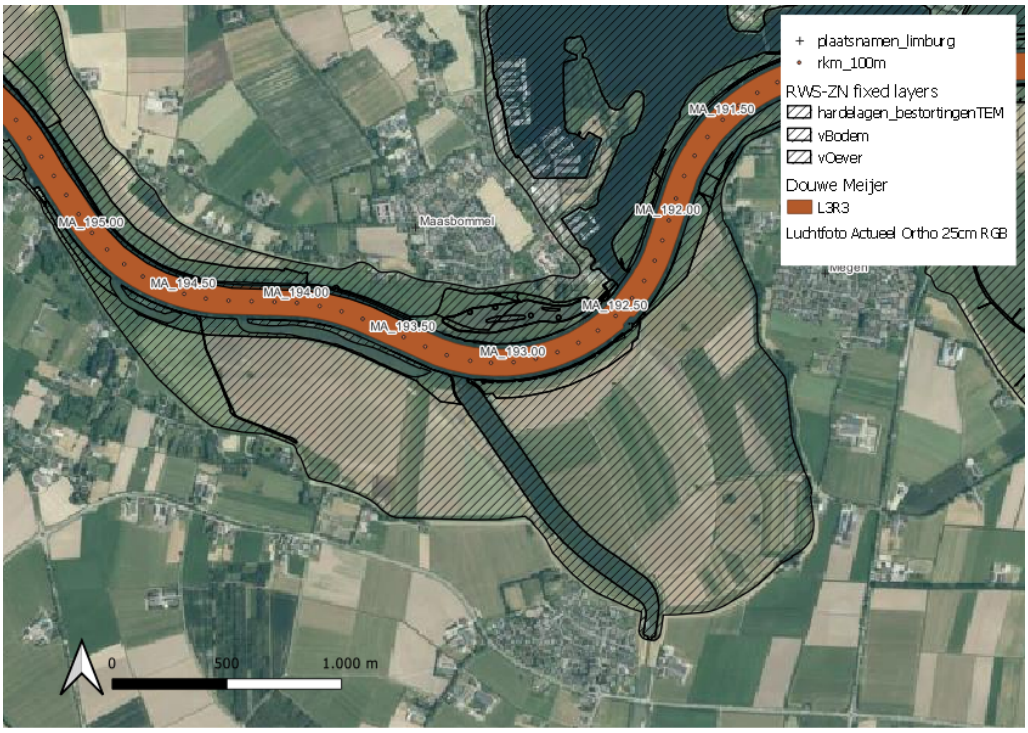

Figure A.7 Sediment availability in the Grave-Lith reach 7/11

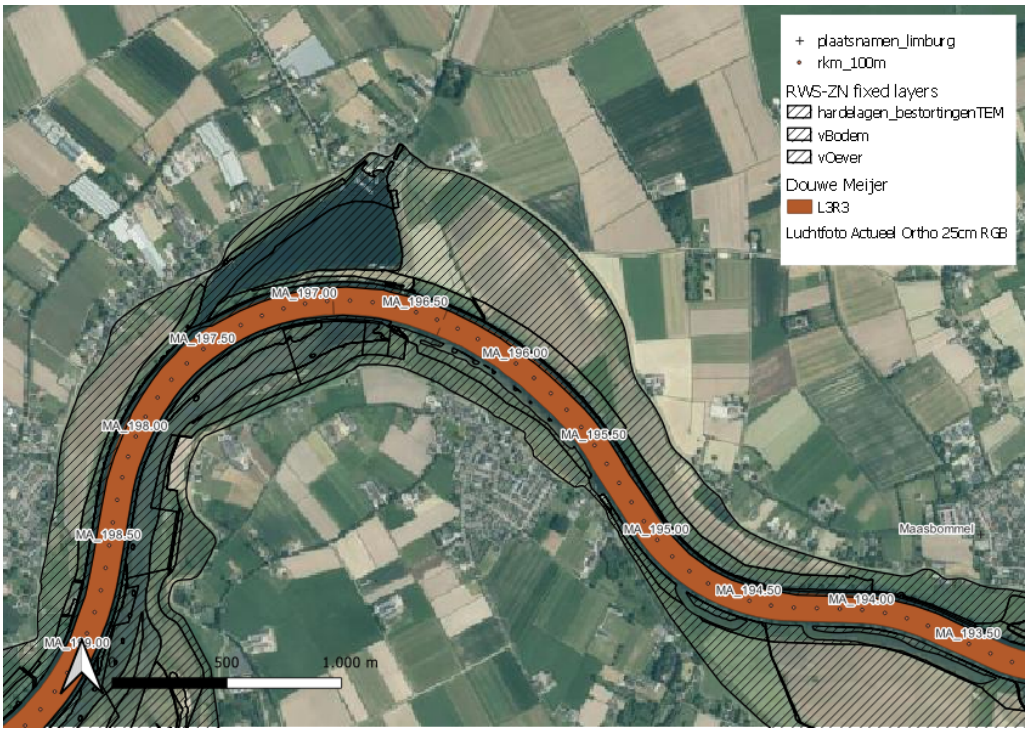

Figure A.8 Sediment availability in the Grave-Lith reach 8/11

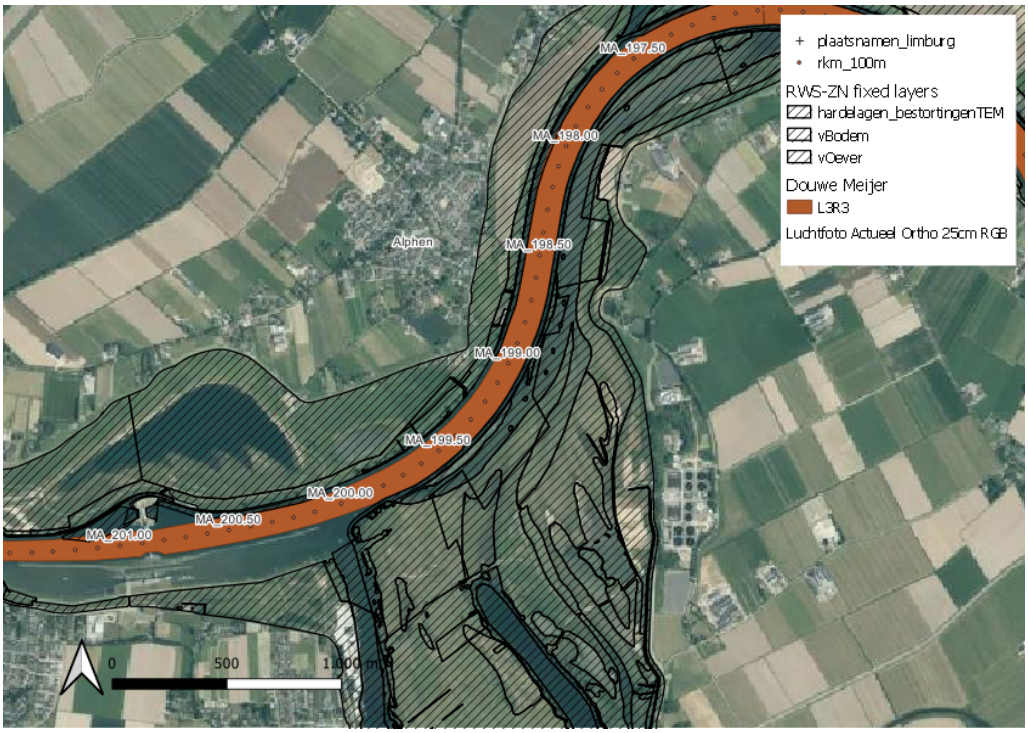

Figure A.9 Sediment availability in the Grave-Lith reach 9/11

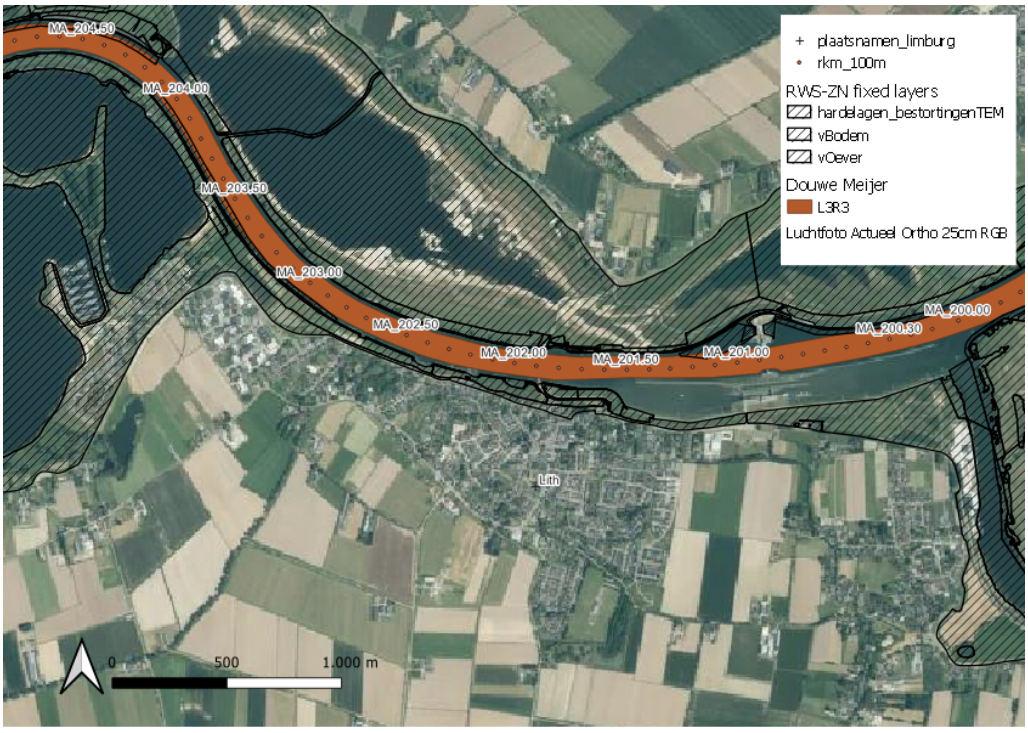

Figure A.10 Sediment availability in the Grave-Lith reach 10/11

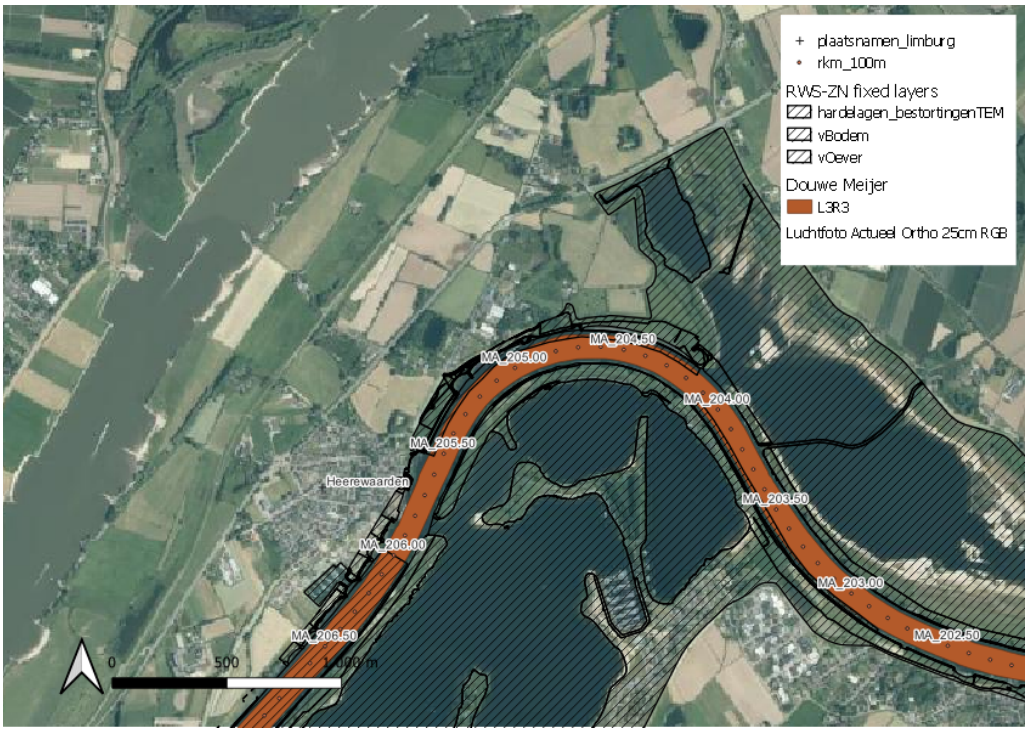

Figure A.11 Sediment availability in the Grave-Lith reach 11/11

Deltares is an independent institute for applied research in the field of water and subsurface. Throughout the world, we work on smart solutions for people, environment and society.

Deltares

www.deltares.nl